Oct 14

Appendix Tokyo Bay storm surge barrier: A conceptual design of the moveable barrier

Kaichen Tian

TU Delft

TABLE OF CONTENTS

1 APPENDIX 1: 2011 TOHOKU EARTHQUAKE

On March 11, 2011 at 14:46 local time, a large earthquake occurred 130 km offshore the north-eastern coast of Japan. According to estimates, this earthquake was of magnitude 9.0 on the Richter scale, which makes it the largest earthquake ever recorded in Japan. The rupture area was 400 km long from north to south and 200 km from east to west. A large amount of strong aftershocks of up to 7.4 on the Richter scale were recorded on the same day in Iwate, Miyagi, Fukushima and Ibaraki prefectures. See Figure 1 and Figure 2.

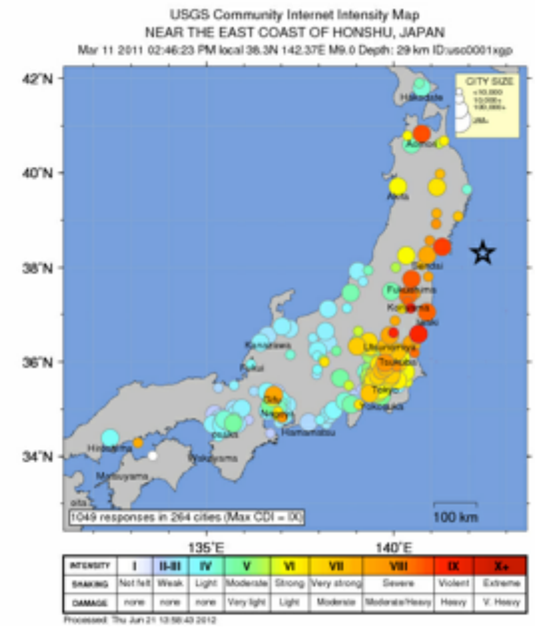

FIGURE 1: MAP OF EARTHQUAKE INTENSITY[1]

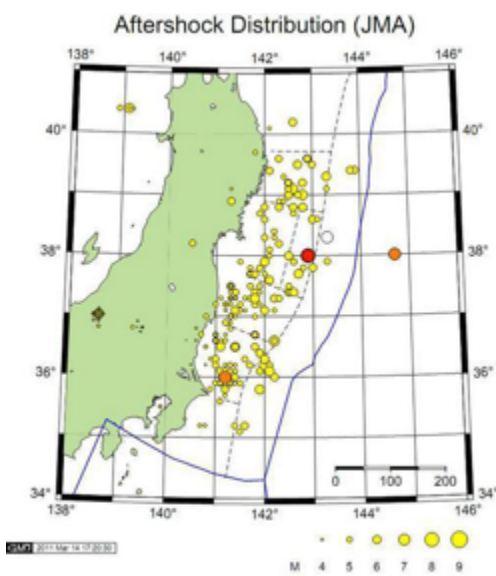

FIGURE 2: AFTERSHOCK DISTRIBUTION[2]

[1] USGS, 2011; http://earthquake.usgs.gov/

[2] Japan Meteorological Agency, 2011; http://www.jma.go.jp

[3] Takahashi et al. 2011, Courtesy of Port and Airport Research Institute, all rights

1.1 The tsunami

The Japan Meteorological Agency issued a tsunami warning three minutes after the main earthquake. Soon after that, a tsunami of 2.6 to 7.7 m was recorded by the GPS mounted buoys at a spot of 100-200 m in water depth off the Tohoku coast. It was expected that a deep-water wave of this magnitude will exceed 10 m in height when reaching coastal areas due to shoaling, while its exact value is very much dependent on the local bathymetry and morphology of the coast. Those huge waves were indeed reaching the north-eastern Japanese coast a few minutes later, affecting approximately 1300 km of the coastline starting from Miyagi, Iwate and Fukushima prefectures, and expanding gradually to the entire north-eastern Japanese coast from Hokkaido in the north to Chiba in the south, The rupture area where the tsunami was generated and the coastal tsunami characteristics in Iwate, Miyagi and Fukushima are shown in Figure 3.

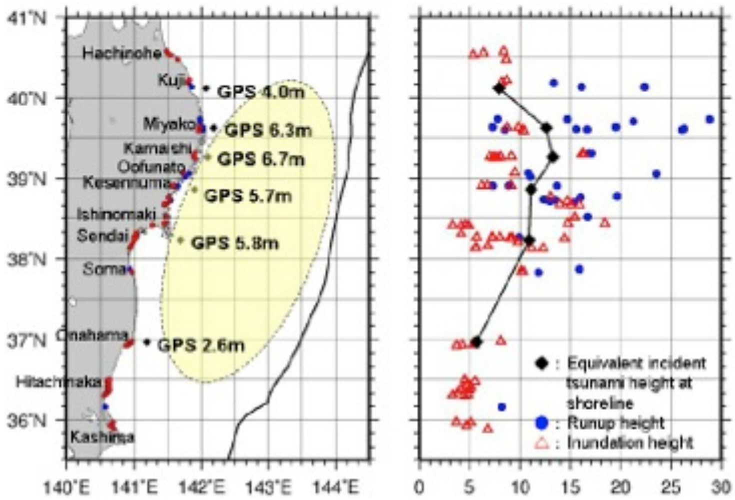

FIGURE 3: LEFT: SOURCE REGION AND GPS OFFSHORE WAVE RECORDS; RIGHT: ESTIMATED INCIDENT TSUNAMI AND MEASURED TSUNAMI MARKS[3]

1.2 The nuclear disaster

Six hours after the earthquake of March 11, a nuclear emergency at Fukushima Daiichi nuclear power plant was reported by the International Atomic Energy Agency. Due to the strong earthquake, the process of shutting down the three operating reactors was automatically initiated. During this process, the water, which is required for the fuel rods in order to cool them down are supplied by the water pumps driven by diesel generators. The operation of the diesel generators failed on the 11th of March, which should have

[2] Japan Meteorological Agency, 2011; http://www.jma.go.jp

[3] Takahashi et al. 2011, Courtesy of Port and Airport Research Institute, all rights reserved

prompted a system of back-up generators to activate, but they did not work due to the tsunami inundation that had damaged the back-up generators. As a consequence, the fuel rods were not sufficiently cooled, and resulted in high pressures in the reactors. On March 12 and at 15:30 local time, a first hydrogen explosion took place, which was followed by two more explosions on the 14th and 15th of March, and a large fire event in a reactor that the empty fuel rods were stored.

As result of those events, a large emission of radiation occurred that has reached 400 millisievert per hour, which is 1.5 million times more than the radiation that a normal human being is supposed to be exposed per hour. The area in a radius of 20 km from the nuclear plant was immediately evacuated after the first explosion. After the second and third explosions, the Japanese authorities took immediate action to cool down the overheated reactors, and to protect contamination of the surrounded region. Also an exclusion zone in a radius of 30 km around Fukushima Daiichi nuclear power station was established.

2 APPENDIX 2: TYPHOONS SIMULATION ON PRESENT AND FUTURE SCENARIOS ON TOKYO BAY

In the past of years numbers of simulations has been done by the Japanese about the typhoon impact on Tokyo Bay. Recent research by S. Hoshino[4] has also included the effect of the climate change and sea level rise into their simulation, showing results for both present and future scenarios, clearly illustrates the conceivable disaster that could be magnified by these effects.

2.1.1.1 The simulation

For this simulation the typhoon of October 1917 is used as reference, which is the worst typhoon to affect Tokyo Bay in the last 100 years. By using this typhoon they have obtained water level elevation for a 1 in 100 year event for present and different future scenarios for different locations in Tokyo Bay. These locations are shown in Figure 4 and Table 1.

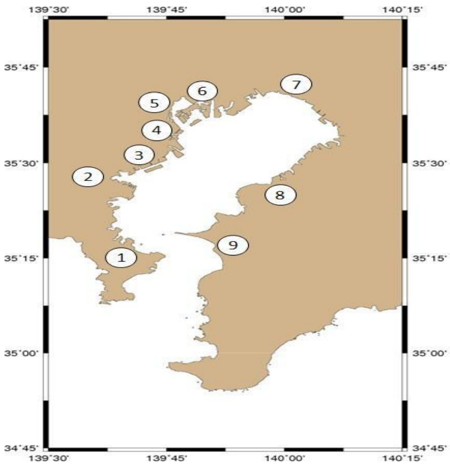

FIGURE 4: LOCATIONS OF INTEREST TOKYO BAY SIMULATION

TABLE 1: LOCATIONS OF INTEREST TOKYO BAY SIMULATION

No	Location	Prefecture
1	Yokosuka	Kanagawa
2	Yokohama	
3	Kawasaki	
4	Samezu	Tokyo
5	Shibaura	
6	Toyosu	
7	Funabashi	Chiba
8	Sodegaura	
9	Futtsu	

For the determination of the minimum central pressure the probability distribution function of Yasuda is used. According to this theory, by the year 2100 a 1 in 100 year typhoon would have a minimum central pressure of 933.9 hPa instead of the historically recorded minimum value of 952.7 hPa.

For the simulation four different future scenarios have been separated regarding the global sea level rise. The first scenario did not consider any sea level rise. This scenario gives insight to the contribution of purely increase of typhoon intensity to flooding risk of Tokyo Bay. The second scenario represents a sea level rise of 0.28 m, which is similar to the lower range presented by the IPCC 4AR. The third scenario is the higher range presented by the IPCC 4AR, which is 0.59 m and the last presented scenario is the more

[4] Sayaka Hoshino, Estimation of Storm Surge and Proposal of the Coastal Protection Method in Tokyo Bay, Waseda University, Feb 2013.

extreme scenario of 1.9 m outlined in Vermeer and Rahmstorf (2009). A summery of the simulated scenarios is given in Table 2.

TABLE 2: SIMULATED SEA LEVEL RISE SCENARIOS

P_0 (Taisho 1917 typhoon)	P_0 (2100, 1 in 100 year storm)	r_{max}	Sea level rise
952.7	933.9	Probability distribution function according to Yasuda et al. (2010b), 10 computations for each scenario	0(cm)
			28(cm)
			59(cm)
			190(cm)

The simulated path of the typhoon is approximately a straight line and the eye of the storm did not through the center of Tokyo Bay, but west of it. This is to ascertain the worst scenario for a 1 in 100 year typhoon. The course of the simulated typhoon is shown in Figure 5.

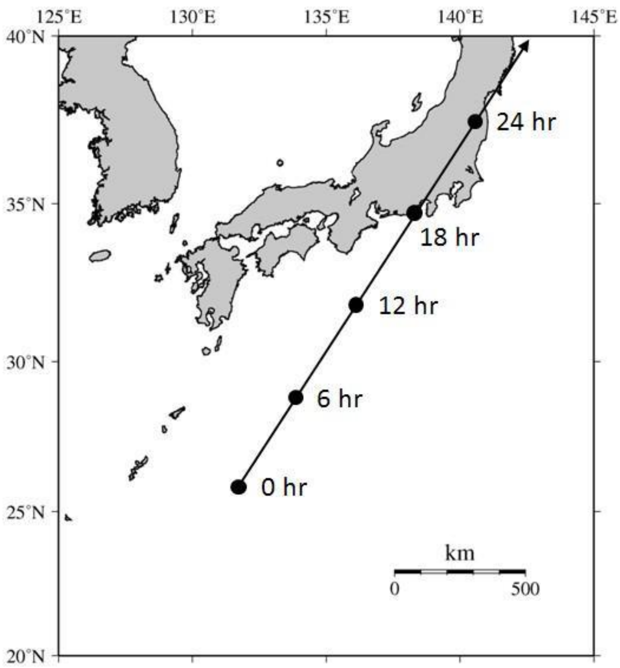

FIGURE 5: PATH SIMULATED TYPHOON

2.1.1.2 Results

The results shown in Figure 6 give the water levels that could be expected for a 1 in 100 year typhoon by the year 2100 at the 9 points of interest after taking into account the intensification of the typhoons due to climate change and a sea level rise of 0.59 m. The vertical axis of the graph represents the frequency of occurrence and the horizontal axis the final water level. The dotted line in this graph shows the level of the current coastal defence in each of these locations.

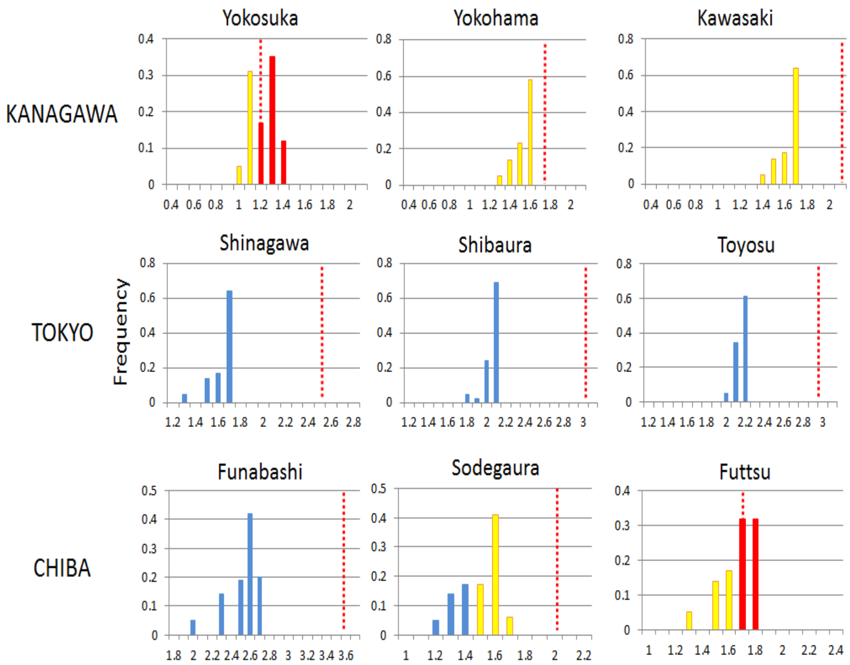

FIGURE 6: FINAL WATER LEVEL BY YEAR 2100 WITH TYPHOON INTENSIFICATION AND A SEA LEVEL RISE OF 0.59 M

In the results of this simulation 2 cases are considered regarding the failure of the coastal defenses, see also Figure 7:

- Case A, the probability that the storm surge will reach a level of at least 50 cm below the top of the defenses.
- Case B, the probability of the storm surge being higher than the protection structures.

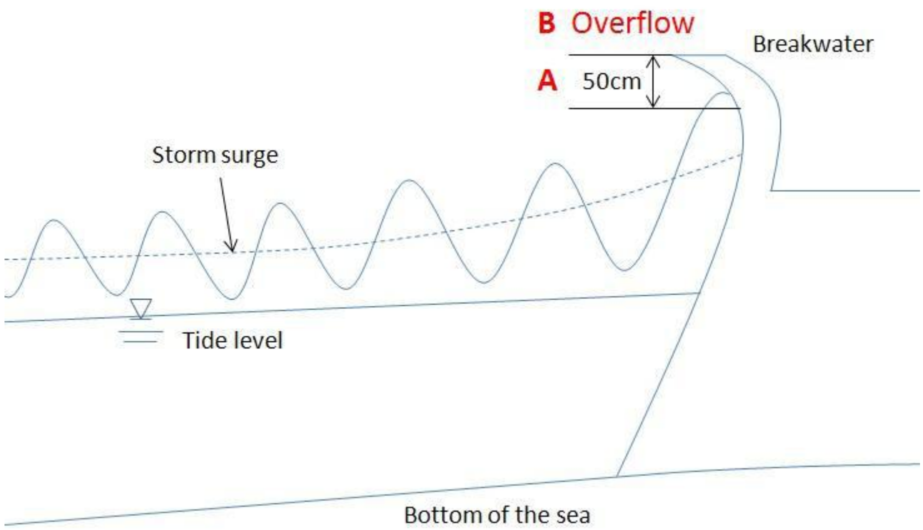

FIGURE 7: CASES A AND B

The probability of each case being reached for each location is presented in Table 3 and Figure 8 shows the cumulative overtopping probabilities for all sea level rise scenarios for case B.

TABLE 3: PROBABILITY (%) THAT THE STORM SURGE HEIGHT BECOMES HIGHER THAN CASE A AND B

Sea level rise	0cm		28cm		59cm		190cm	
Level of Storm Surge Height	A	B	A	B	A	B	A	B
Yokosuka	12	0	95	0	100	64	100	100
Yokohama	0	0	58	0	100	0	100	100
Kawasaki	0	0	64	0	100	0	100	100
Samezu	0	0	0	0	0	0	100	100
Shibaura	0	0	0	0	0	0	100	100
Toyosu	0	0	0	0	0	0	100	100
Funabashi	0	0	0	0	0	0	100	81
Sodegaura	0	0	0	0	64	0	100	100
Futtsu	0	00	81	0	100	64	100	100

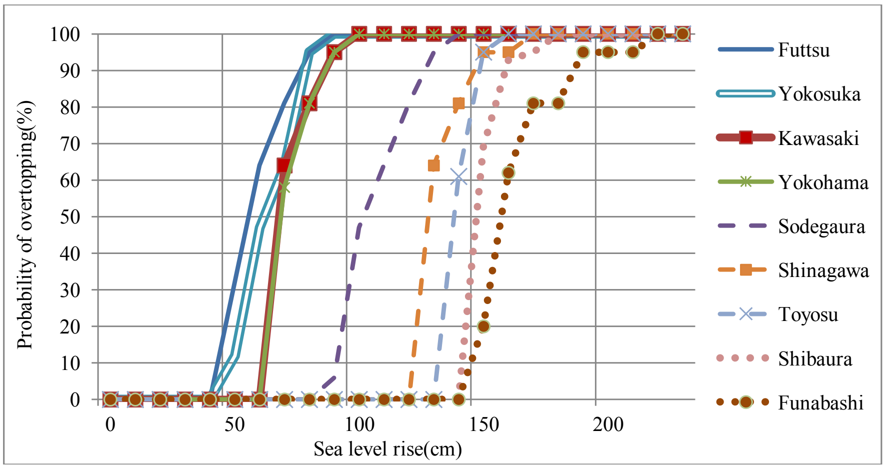

FIGURE 8: CUMMULATIVE OVERTOPPING PROBABILITY OF SEA DEFENSES (CASE B) IN EACH SEA LEVEL RISE SCENARIO FOR A 1 IN 100 YEAR TYPHOON BY THE YEAR 2100

2.1.1.3 Economic damage

Tokyo city has a population of around 13 million inhabitants and is the city with the greatest GDP in the world with a gross output of 1.479 billion dollars. Together with adjacent cities such as Yokohama and Kawasaki it forms what it is called the 'greater Tokyo', having a total population of more than 35 million people, making it the largest megalopolis in the world. Therefor a typhoon flooding of the area will not only have a great impact on the Japanese economy, but also the world economy. The potential areas at risk of inundation along Tokyo Bay in Tokyo, Kanagawa and Chiba prefectures are shown in Figure 9, Figure 10 and Figure 11. The maps are based on elevation maps of Tokyo Bay and include the effect of the intensification of the future typhoons together with a sea level rise of 0.59 m and 1.90 m. The extent of the inundation area after dyke failure is represented by two contour lines. The thick blue line represents the future scenario with a sea level rise of 0.59 m and the light blue line represents the scenario with 1.90 m sea level rise. The maximum water levels shown in the maps are considered to take place at maximum high tide (+ 0.966 T.P.) and have included the mean expected storm surge height and the sea level rise for each scenario. The water levels are expressed at Tokyo Pail (T.P.). Due to the relative small population density in Chiba, the economic damage analysis has only included the Tokyo and Kanagawa prefectures, which the latter includes Yokohama and Kawasaki.

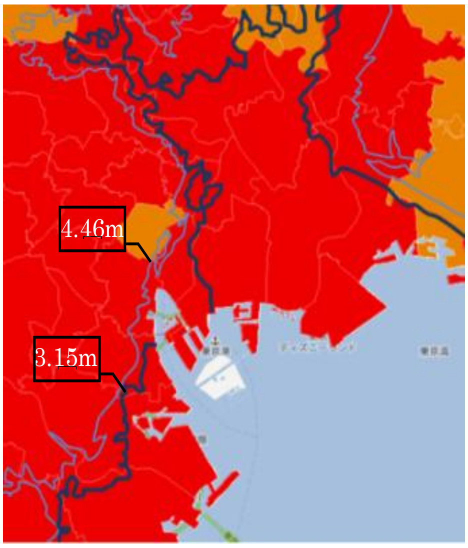

FIGURE 9: INNUNDATION AREA TOKYO FOR 1 IN 100 YEAR TYPHOON BY YEAR 2100 FOR 0.59 AND 1.90 M SEA LEVEL RISE

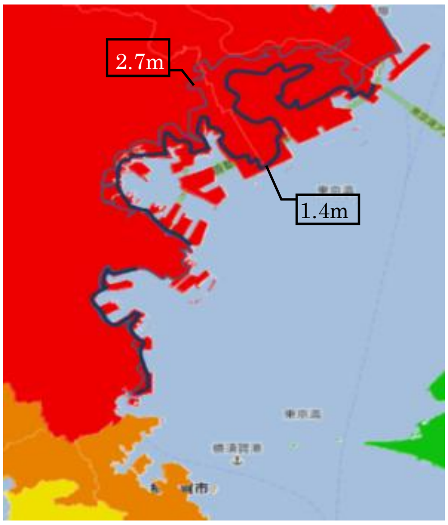

FIGURE 10: INNUNDATION AREA KANAGAWA FOR 1 IN 100 YEAR TYPHOON BY YEAR 2100 FOR 0.59 AND 1.90 M SEA LEVEL RISE

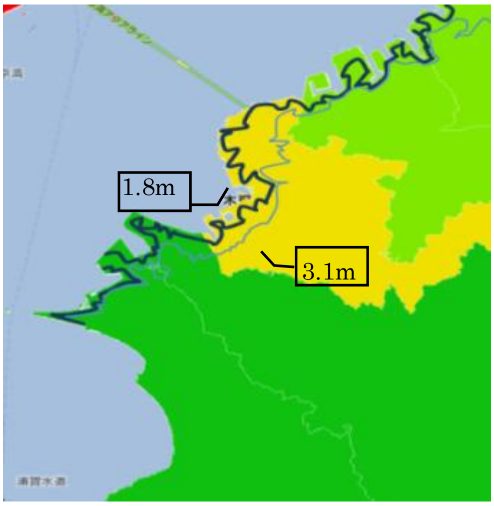

FIGURE 11: INNUNDATION AREA CHIBA FOR 1 IN 100 YEAR TYPHOON BY YEAR 2100 FOR 0.59 AND 1.90 M SEA LEVEL RISE

The economic damage in the Tokyo and Kanagawa prefectures is calculated by adding up all the damage in the inundated areas. Figure 12 shows the damage for inundation levels up to +4.5 m T.P. in Tokyo and +4.0 m T.P. in Kanagawa. In the figure the 0 m indicates no dyke failures and therefor the area inside the dyke would be dry. It is important to note that some areas in Tokyo are under mean sea level; so even at present they will suffer damage if the dyke break.

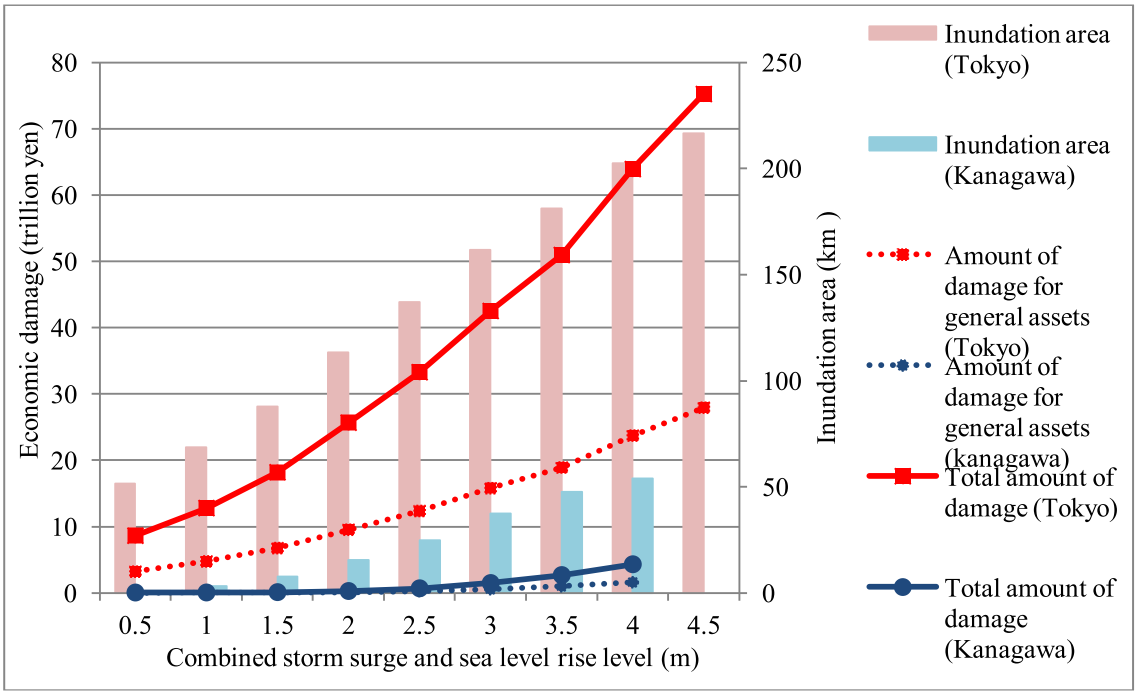

FIGURE 12: ECONOMIC DAMAGE TOKYO AND KANAGAWA FOR DIFFERENT INNUNDATION LEVELS

3 APPENDIX 3: RAISE/BUILD COASTAL DYKES

The cost of raising costal dykes for a 1 in 100 year typhoon and a sea level rise of 1.9 m has also been investigated by S. Hoshino. This estimation has been done for the following sub-measures:

- Raise dyke heights
- Build new dykes
- Anti-earthquake reinforcements
- Raise ground level

These measures are investigated for the Tokyo, Kawasaki and Yokohama region. They are undertaken such that the risk levels in the 2100 are similar to those in 2010 for a 1.9 m sea level rise scenario. A summary of the addaption measures for diffrent regions is given in Table 4.

TABLE 4: SUMMARY OF ADDAPTION MEASURES TO BE UNDERTAKEN IN TOKYO AND KANAGAWA TO ENSURE THAT RISK LEVELS IN THE YEAR 2100 ARE SIMILAR TO THOSE IN 2010 FOR A 1.9 M SEA LEVEL RISE SCENARIO.

		Measures for areas protected by coastal dykes			Measure for areas outside of coastal dykes
		Raise dyke height	Build a new dyke	Anti-earthquake Reinforcement	Raise the ground level
Tokyo	Tokyo port	○	○	○	○
Kanagawa	Kawasaki port	○	○	○	○
	Yokohama port	×	○	○	○

Locations of dykes that would require rising or rebuilding are shown in Figure 13, Figure 14 and Figure 15.

FIGURE 13: LOCATION OF DYKES THAT WOULD REQUIRE RISING OR REBUILDING IN TOKYO FOR A 1.9 M SEA LEVEL RISE SCENARIO. DIFFERENT LETTERS CORRESPROND TO DIFFERENT TYPES OF DYKES.

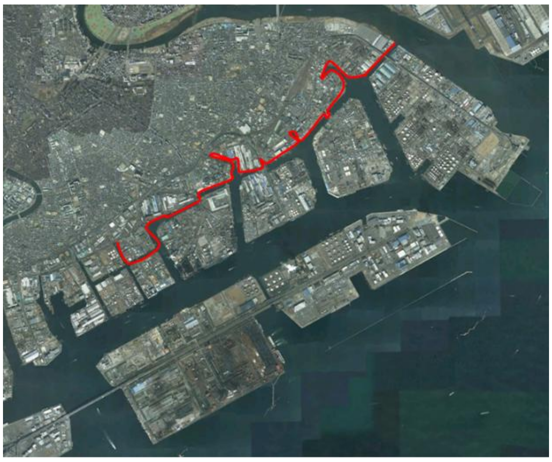

FIGURE 14: LOCATION OF DYKES THAT WOULD REQUIRE RISING OR REBUILDING IN KAWASAKI FOR A 1.9 M SEA LEVEL RISE SCENARIO.

FIGURE 15: LOCATION OF DYKES THAT WOULD REQUIRE RISING OR REBUILDING IN YOKOHAMA FOR A 1.9 M SEA LEVEL RISE SCENARIO. NOTE THAT CURRENTLY THE PORT AREA OF YOKOHAMA IS MOSTLY UNPROTECTED (TO THE SOUTH, MARKED WITH NUMBER 2 IN THE MAP).

The cost of these dyke raising/rebuilding measures are investigated individually and given in the following tables.

TABLE 5: TOTAL COSTS OF RAISING THE DYKES IN TOKYO AND KAWASAKI, ASSUMING A 1.9 M SEA LEVEL RISE SCENARIO

	Tokyo	Kawasaki
Length	45.9km	13.5km
Height of storm surge (in T.P.)	4.5m	4.0m
Cost (100 million yen)	0.58	0.22

TABLE 6: TOTAL COSTS OF BUILDING NEW COASTAL DYKES IN TOKYO, KAWASAKI AND YOKOHAMA, ASSUMING A 1.9 M SEA LEVEL RISE SCENARIO, EXCLUDING INDIRECT COSTS.

	Tokyo	Kawasaki	Yokohama
Length	22.0 km	13.5 km	21.4 km
Height (T.P.)	4.5m	4.0 m	3.9m
Cost (bn yen)	6.01	3.63	5.78

TABLE 7: TOTAL COSTS OF ANTI EARTHQUAKE REINFORCEMENT FOR NEW COASTAL DYKES IN TOKYO, KAWASAKI AND YOKOHAMA, ASSUMING A 1.9 M SEA LEVEL RISE SCENARIO, EXCLUDING INDIRECT COSTS.

	Tokyo	Kawasaki	Yokohama
Length	22.0 km	13.5 km	21.4 km
Cost (bn yen)	97.4	59.7	94.78

Except for the coastal dykes, some areas outside the coastal defence such as port facilities also need to be raised. The distribution of these areas is shown in Figure 16, Figure 17 and Figure 18. The cost estimation required for this measure is given in Table 8

FIGURE 16: DISTRIBUTION OF PORT FACILITIES AND OTHER AREAS OUTSIDE COASTAL DEFENCES THAT WOULD REQUIRE RAISING IN TOKYO FOR A 1.9 M SEA LEVEL RISE SCENARIO

FIGURE 17: DISTRIBUTION OF PORT FACILITIES AND OTHER AREAS OUTSIDE COASTAL DEFENCES THAT WOULD REQUIRE RAISING IN KAWASAKI FOR A 1.9 M SEA LEVEL RISE SCENARIO.

FIGURE 18: DISTRIBUTION OF PORT FACILITIES AND OTHER AREAS OUTSIDE COASTAL DEFENCES THAT WOULD REQUIRE RAISING IN YOKOHAMA FOR A 1.9 M SEA LEVEL RISE SCENARIO.

TABLE 8: TOTAL COSTS OF RAISING PORT FACILITIES AND OTHER AREAS OUTSIDE COASTAL DYKES IN TOKYO, KAWASAKI AND YOKHAMA, ASSUMING A 1.9 M SEA LEVEL RISE SCENARIO. NOTE THAT THE COST OF DEMOLISHING AND REBUILDING INSTALLATIONS IS NOT INCLUDED.

	Tokyo	*Kawasaki*	*Yokohama*
Area	11.9 km	17.6 km	8.5 km
Height (T.P.)	4.5 m	4.0 m	3.9 m
Cost (bn yen)	19.51	67.73	34.52

A summary of e adaption measure components for each location is given in Table 9 and the total costs of adapting old dykes or building new dykes is given in Table 10.

TABLE 9: SUMMARY OF ADAPTION MEASURE COMPONENTS FOR EACH LOCATION, FOR A 1.9 M SEA LEVEL RISE SCENARIO.

		Measures for coastal dykes (bn yen)			Measures for areas outside dykes (bn yen)
Prefecture	Location	① Raise dykes height	② Build new dykes	③ Anti-earthquake Reinforcement	④ Raise the ground level
Tokyo	Tokyo port	0.58	6.01	97.43	19.51
Kanagawa	Kawasaki port	0.22	3.63	59.78	67.79
	Yokohama port	×	5.78	94.77	34.52

TABLE 10: TOTAL COSTS OF ADAPTING OLD DYKES OR BUILDING NEW ONES FOR A 1.9 M SEA LEVEL RISE SCENARIO.

	①+③+④ Adapting old dykes (bn yen)	②+③+④ Building new dykes (bn yen)
Tokyo	117.5	123.0
Kanagawa	257.1	266.3

4 APPENDIX 4: TYPHOON BARRIER SIMULATION TOKYO BAY

In 1964 a simulation has been done by Takeshi Ito for the storm surge height reduction by a typhoon barrier in Tokyo Bay. The simulated typhoon is the typhoon that has caused the most sever damage for the Japanese history, named the Ise-Bay Typhoon in 1959.

4.1.1.1 The model configuration

The path of the typhoon is assumed to proceed northward along a course parallel to the axis of the Tokyo Bay with a propagation speed of 73 km/h. The eye of the storm is assumed to be 40 km west of Tokyo, see Figure 19. The considered worst-case scenario course is the A-course and only this course will be considered in this report. This is to ensure a worst-case scenario for this typhoon. The simulated barrier is constructed across the central part of Tokyo Bay, having a length of circa 18 km, see Figure 20. The barrier is simulated on the central part instead of at the mouth of the bay. This is because a check on the effectiveness of the two positions for the storm surge reduction has already been made, concluding that the central position is more effective than the other. An opening for navigation is included in the barrier model. From the standpoint of navigation, it is preferable to have a wide opening. On the other hand, wide opening will decrease the effect of the barrier on the storm surge reduction. Therefor a series of simulations with different opening width had been carried out and are listed below:

1) No barrier
2) Central opening width 2000 m
3) Central opening width 1000 m
4) Central opening width 500 m

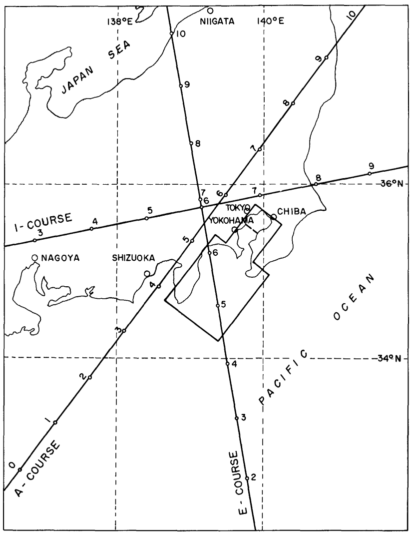

FIGURE 19: COURSE OF THE SIMULATED TYPHOON

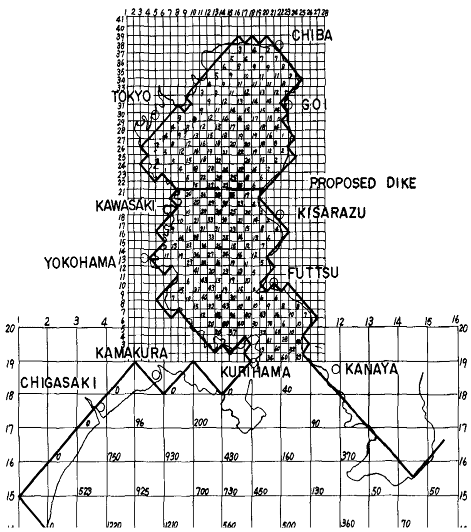

FIGURE 20: LOCATION SIMULATED BARRIER

4.1.1.2 Results

Several relevant results from this simulation are shown in the figures below. It can be seen that the barrier is showing significant storm surge reduction of about 0.4 - 0.7 m already for the inner part of the barrier if the opening is 1000 m and no significant surge rise for the locations outside the barrier. According to this simulation the superposition of the high tide level and the storm surge gives an overestimation of the final water level. Notice that this simulation is done 50 years ago, sea level have been rising in these 50 years and together with the possible typhoon intensification and further sea level rise, the absolute water level for a typhoon with the same return period as Ise-Bay typhoon will be higher in the future. But this simulation does give a good indication about the effectiveness of a storm surge barrier in Tokyo Bay.

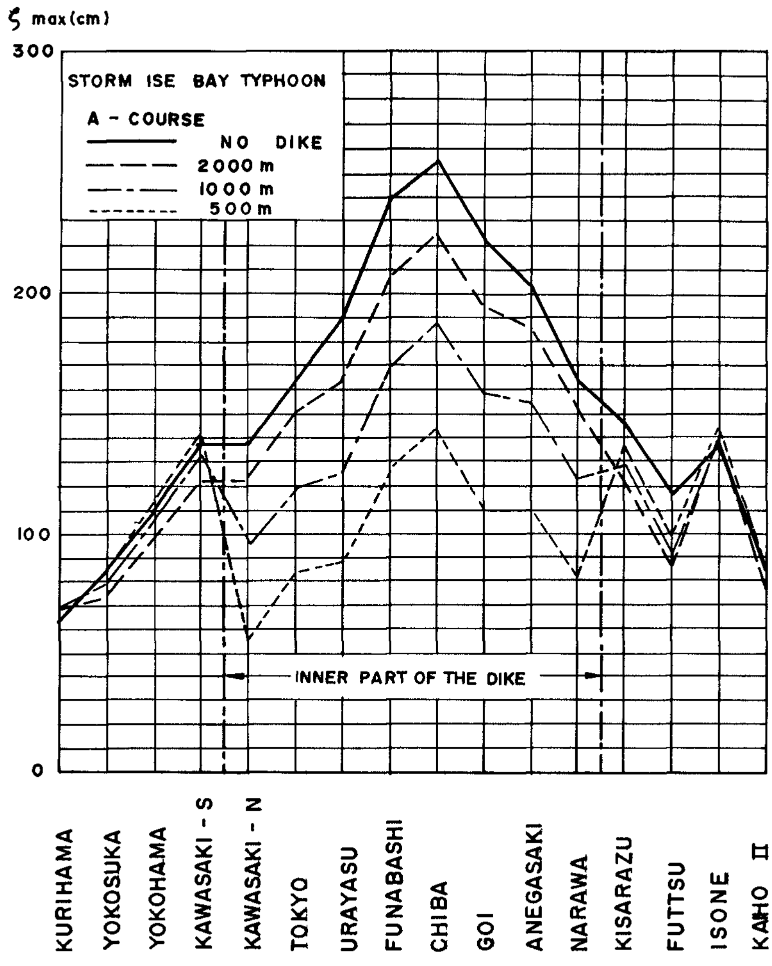

FIGURE 21: CALCULATED MAXIMUM SURGE ELEVATION ISE-WAN TYPHOON FOR DIFFERENT BARRIER OPENING WIDTHS (A-COURSE)

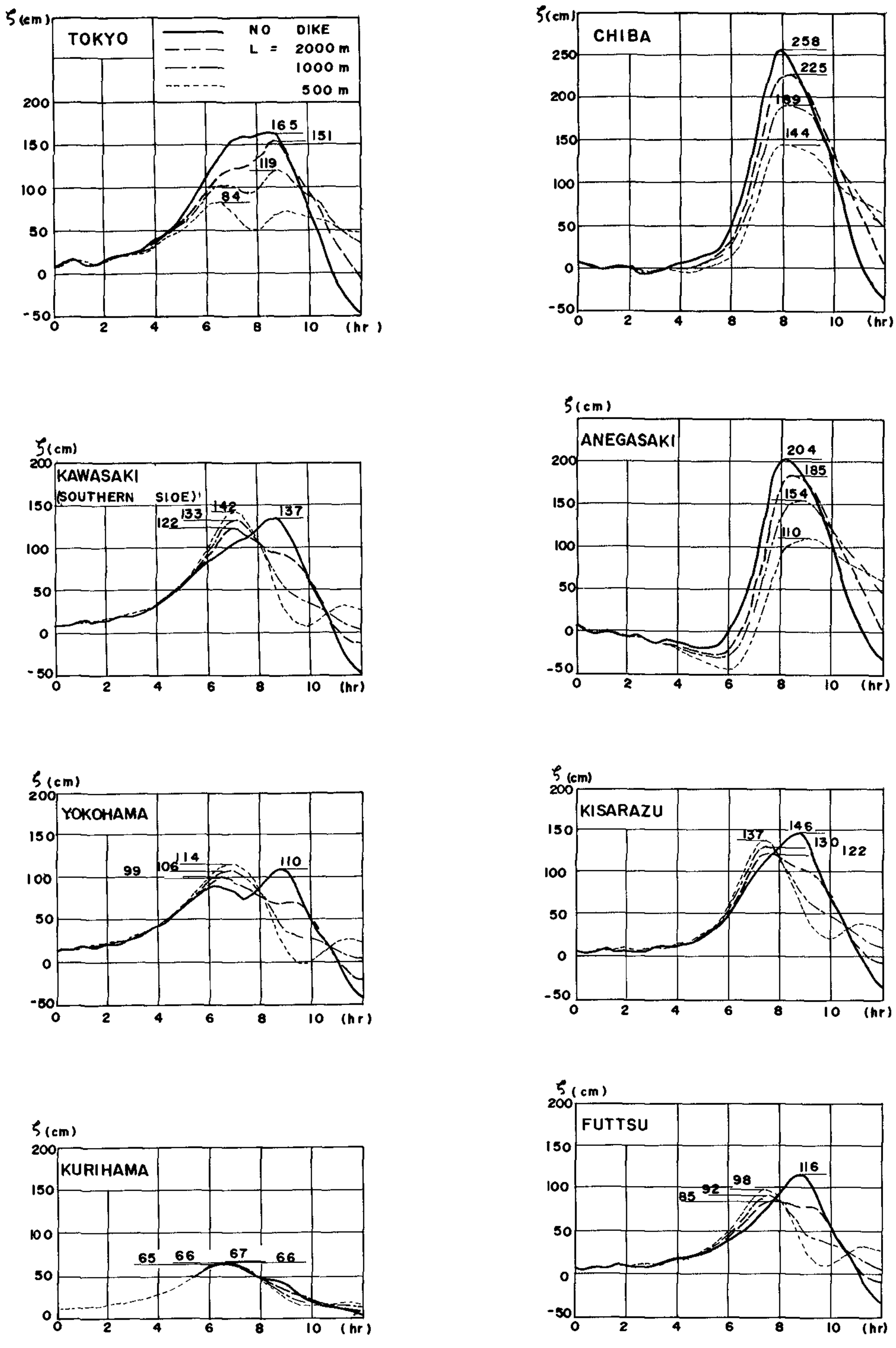

FIGURE 22: PREDICTION OF WATER LEVEL AT VARIOUS POINTS SHOWING THE EFFECT OF THE BARRIER ON SURGE REDUCTION FOR DIFFERENT OPENING WIDTH

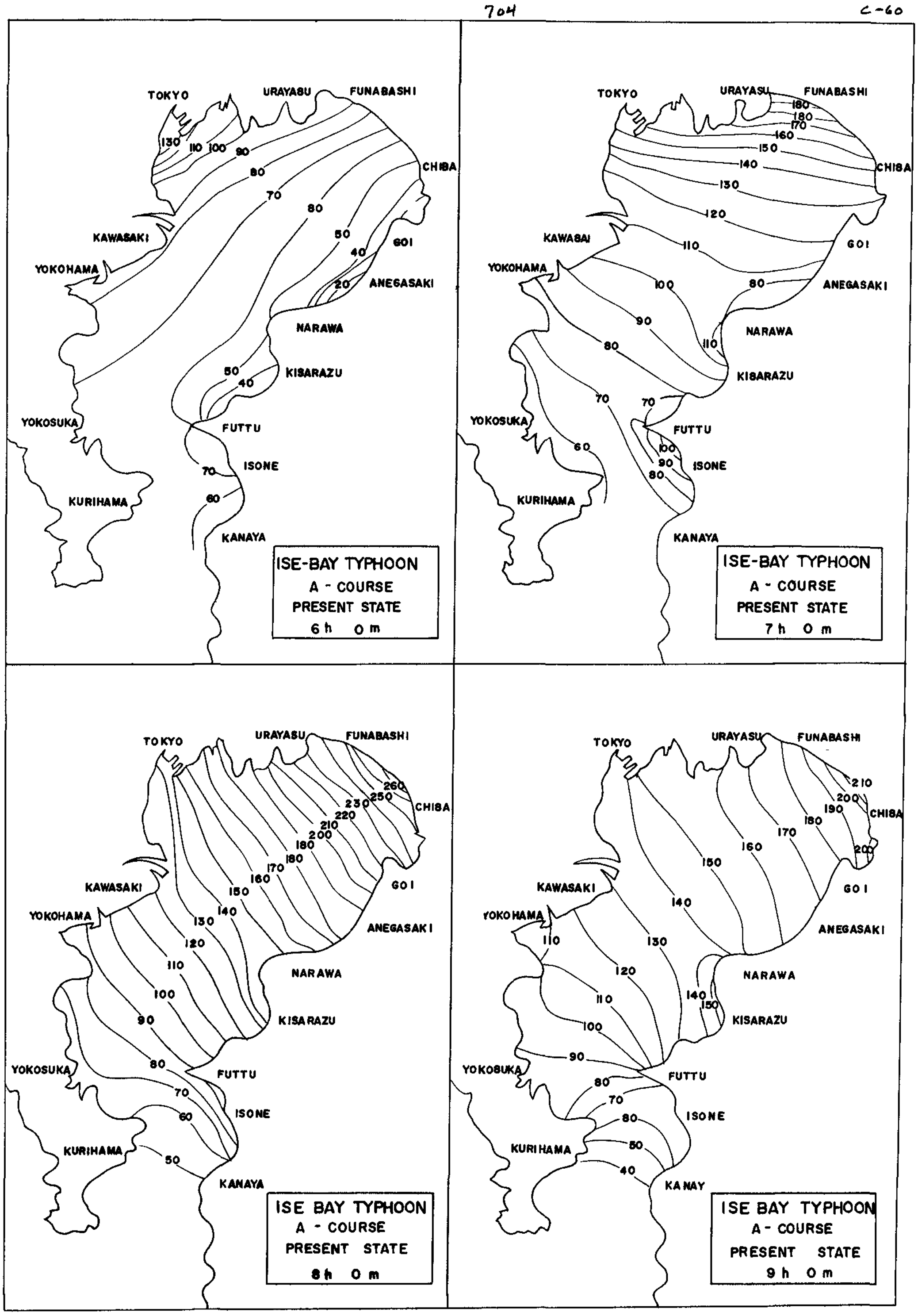

FIGURE 23: COUTOUR LINE SEA LEVEL ELEVATION DUE TO STORM SURGE CAUSED BY ISE-BAY TYPHOON WITHOUT BARRIER

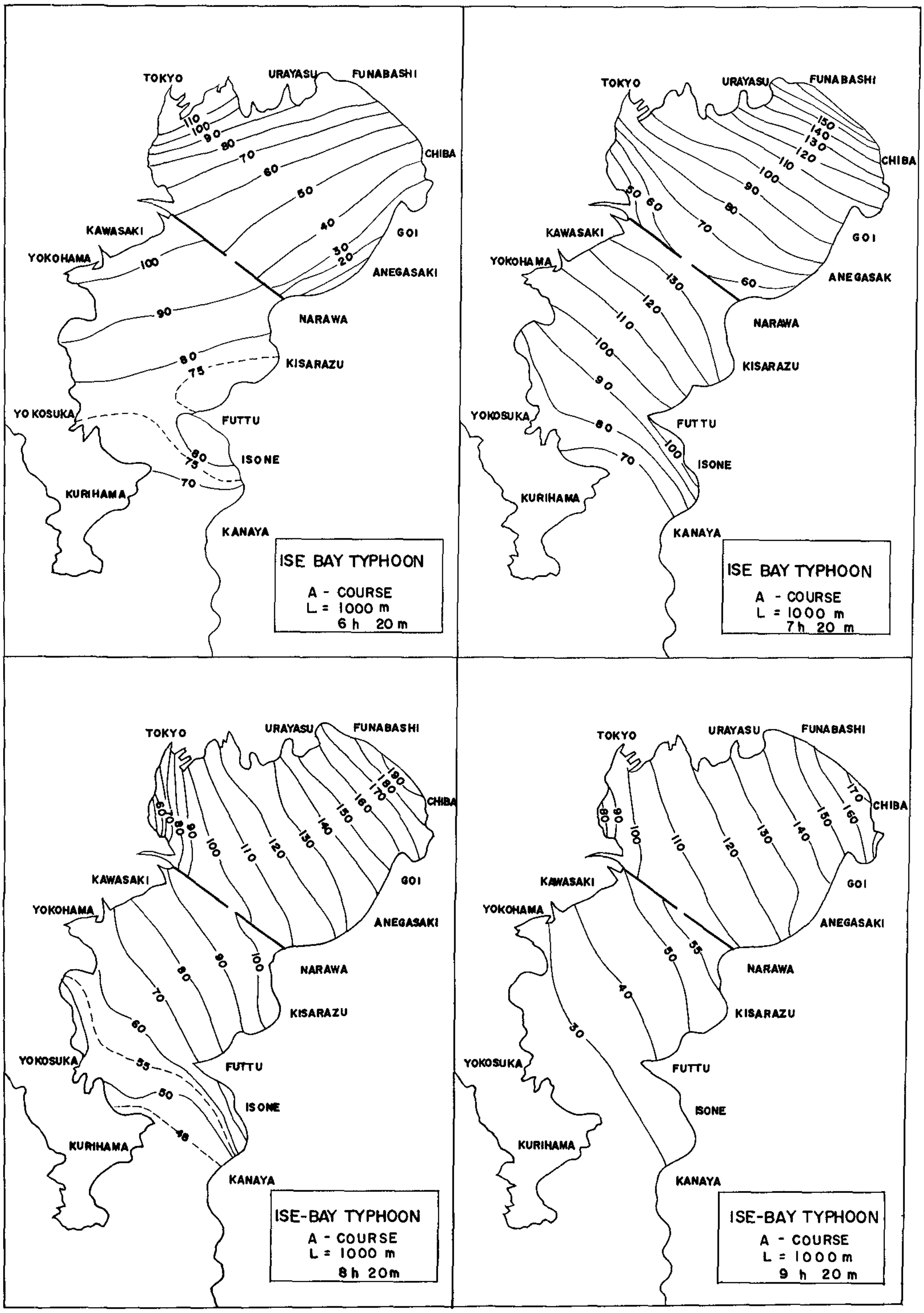

FIGURE 24: COUTOUR LINE SEA LEVEL ELEVATION DUE TO STORM SURGE CAUSED BY ISE-BAY TYPHOON WITH BARRIER

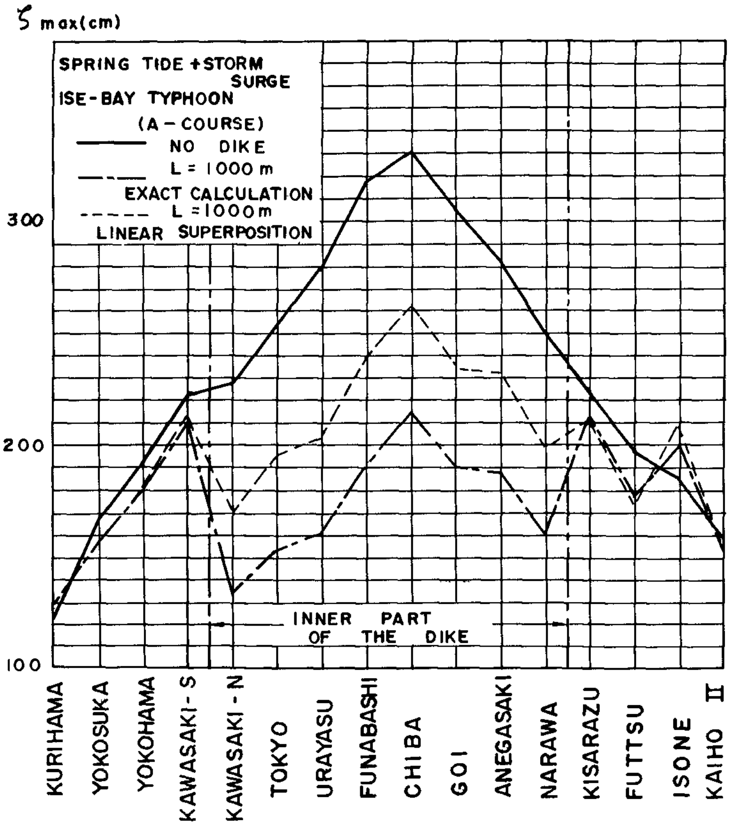

FIGURE 25: FINAL WATER LEVEL (INCLUDE DAILY TIDE), THE LINEAR SUPERPOSITION OF THE TIDE GIVE AN OVEREXTIMATION OF THE WATER LEVEL ACCORDING TOT HIS SIMULATION.

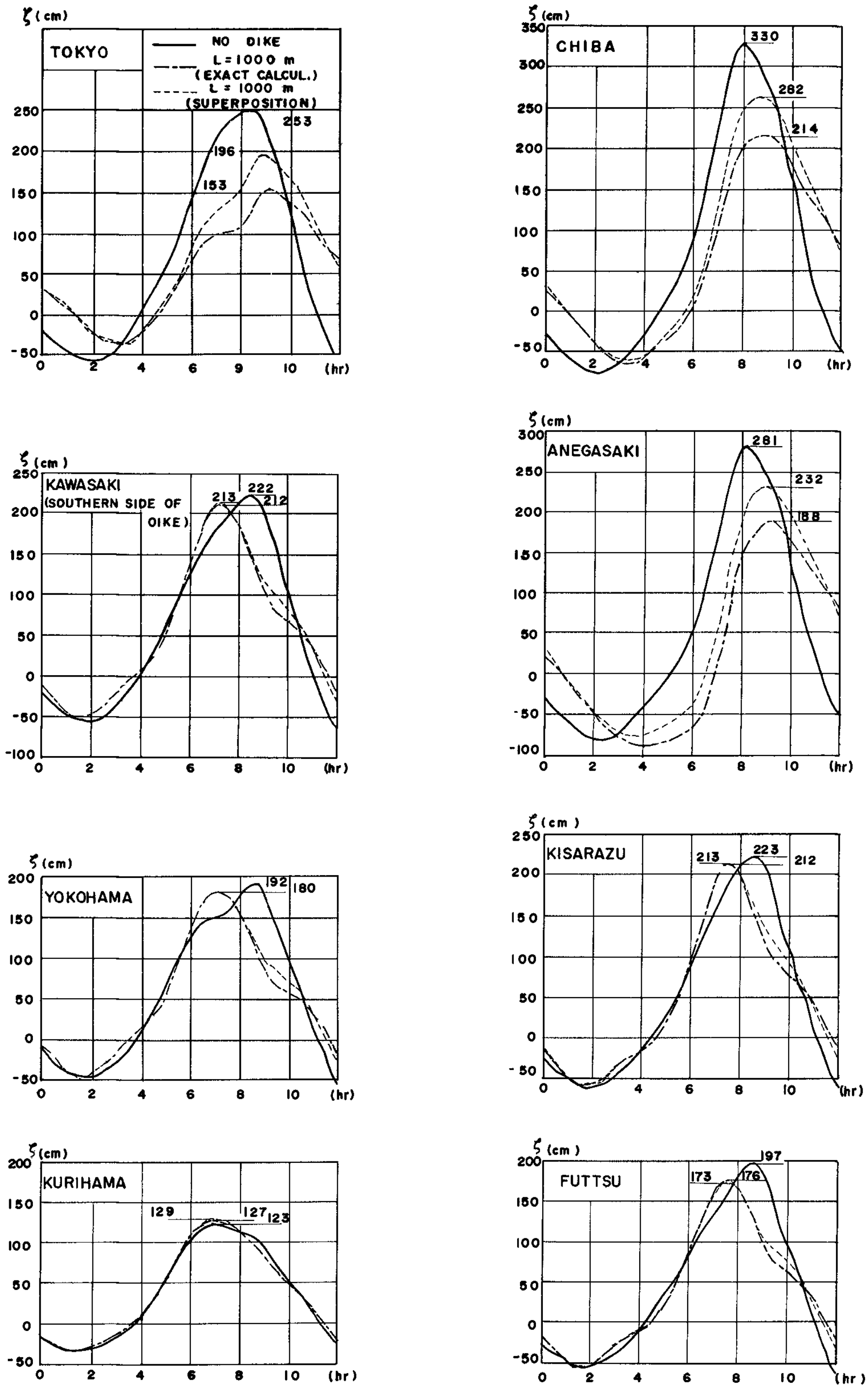

FIGURE 26: FINAL WATER LEVEL (INCLUDE DAILY TIDE) SHOWN FOR VARIOUS LOCATIONS, THE LINEAR SUPERPOSITION OF THE TIDE GIVE AN OVEREXTIMATION OF THE WATER LEVEL ACCORDING TOT HIS SIMULATION.

5 APPENDIX 5 : BARRIER LOCATION

To be able to find the most optimal location, 5 possible barrier locations are presented in Figure 27 and the subsoil of the bay is presented in Figure 28. The bathymetries of the considered barrier locations are shown in Figure 29 to Figure 33. They are based on a depth contour map provided by Miguel Estaban (personal communication).

FIGURE 27: POSSIBLE BARRIER LOCATIONS

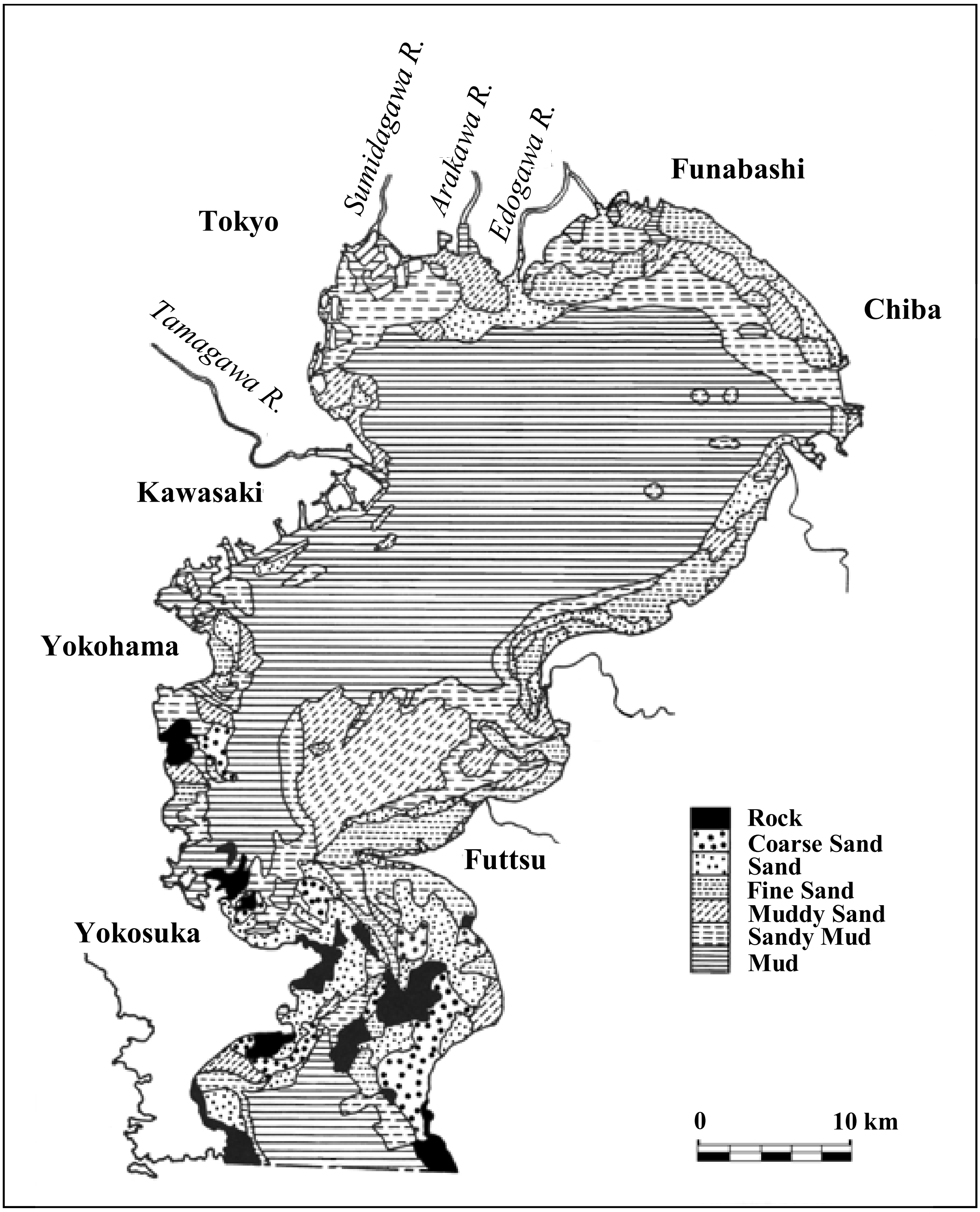

FIGURE 28: SUBSOIL MAP TOKYO BAY (REFERENCE: PERSONAL COMMUNICATION MIGUEL ESTEBAN)

5.1.1 BARRIER LOCATION 1

This location is approximately the same location as described by the simulation done by Takeshi Ito. Because of the existing tunnel in the location suggested in the simulation, the proposed location 1 for the barrier will be at about 2 km south-west of the original location.

Despite the fact that this location has the most shallow bathymetry of al the considered locations, shown in Figure 29, and the high effectiveness in surge height reduction at Tokyo shown in the simulation in chapter 3.2.4, it has the larges to be closed cross-section and span of all the locations, which is around 310000 m² and 14 km respectively, making it probably the most expensive location to close. The subsoil of this location contains mainly mud, see Figure 28, which is relatively weak material. Also it leaves Yokohama, which is the second largest city in Japan, outside the protected area. Since a lot of the Japanese industrial is concentrated in Yokohama, it bears a very large value for the Japanese economy and will certainly grow larger in the coming 100 years.

Advantage
- High effectiveness in surge height reduction at Tokyo
- Most shallow bathymetry of the considered locations

Disadvantage
- Largest to be closed cross-section, around 310000 m²
- Longest span, around 14 km
- No protection to Yokohama
- Relatively weak subsoil (mud)

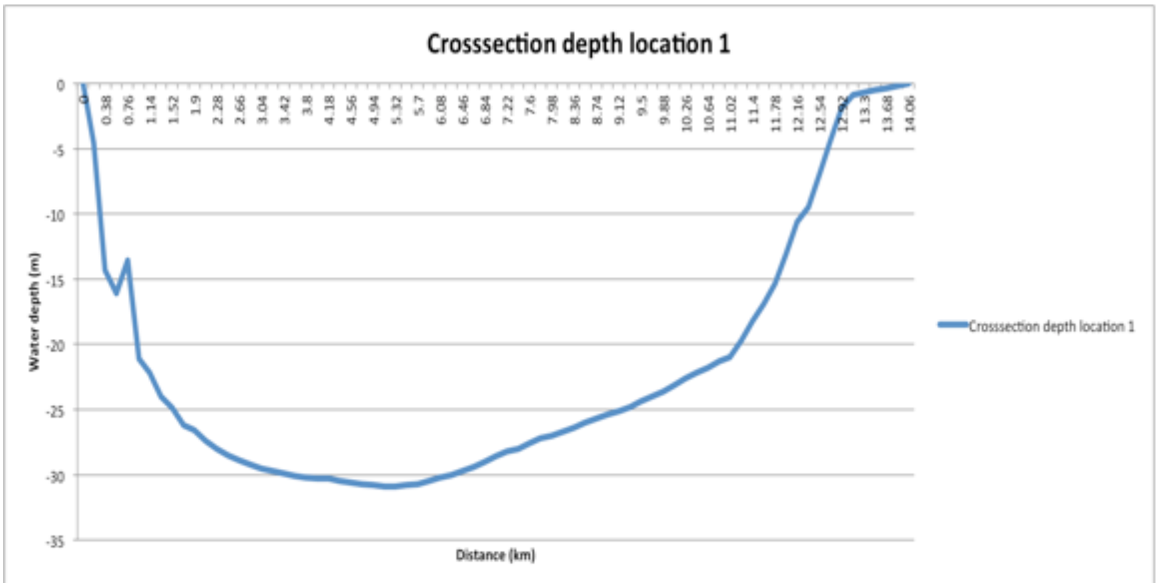

FIGURE 29: BATHYMETRY BARRIER LOCATION 1

5.1.2 BARRIER LOCATION 2

This barrier location protects both Tokyo and Yokohama, but has the longest span of all the considered barrier locations, which is around 10.5 km. It has a 'to be closed' area of around 260000 m^2 and the deepest part of this location is around 52 m. This depth avoids the deep split at the mouth of the Bay and is therefore shallower than the depth of the deepest breakwater in the world (Kamaishi breakwater) with a depth of 63 m. The subsoil of this location contains both sand and mud.

Advantage

- Protection Yokohama
- Avoiding deep split at the mouth
- Less deep compared to the similar location 3

Disadvantage

- Longest span of all the considered barrier locations, 10.5 km
- Despite avoiding the deep split, still deep bathymetry

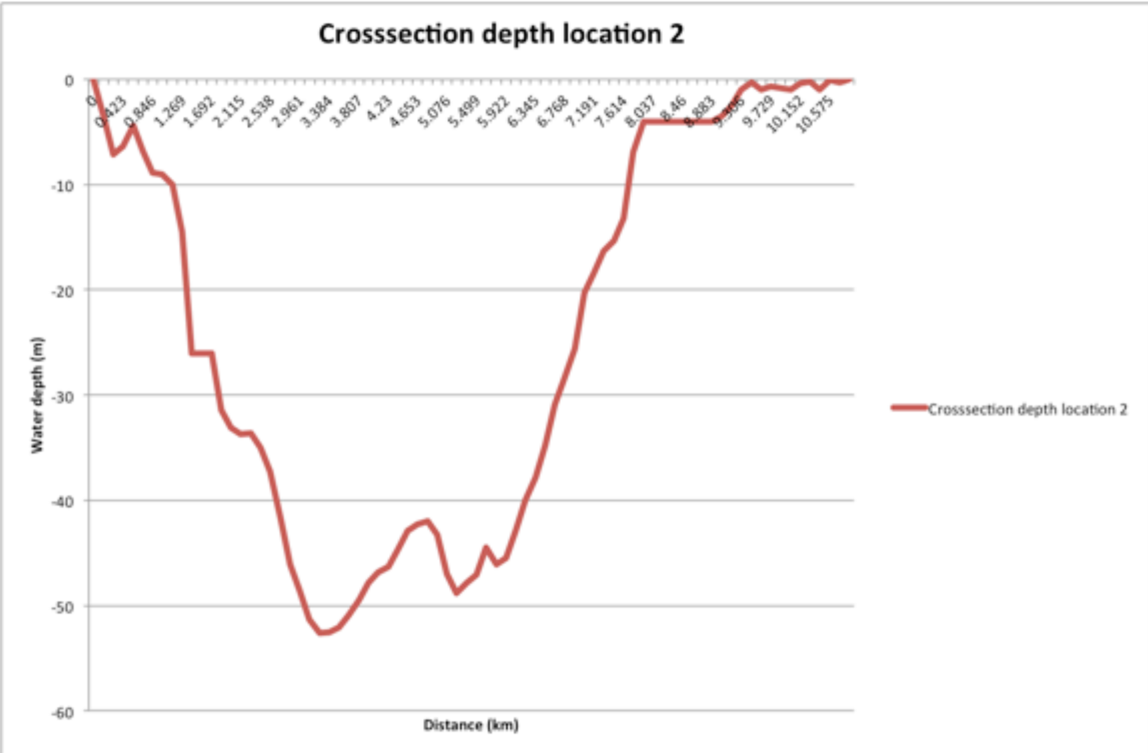

FIGURE 30: BATHYMETRY BARRIER LOCATION 2

5.1.3 BARRIER LOCATION 3

This barrier location is almost the same as the previous location; only this location has a shorter span, which is around 9.5 km. But due to the greater depth of this location (58 m) compared to location 2 it has approximately the same 'to be closed area' as location 2. Both location 2 and 3 protects Yokohama and avoids the deep split. The reason to consider both barrier location 2 and 3 is to compare the suitability of both bathymetries to build the barrier. The subsoil of this location contains both sand and mud; a small part of is rock.

Advantage

- Protection Yokohama
- Avoiding deep split at the mouth
- Flatter bottom compared to location 2, which makes it more suitable for constructions

Disadvantage

- Despite avoiding the deep split, still deep bathymetry
- Deeper bathym `etry compared to the similar location 2

FIGURE 31: BATHYMETRY BARRIER LOCATION 3

5.1.4 BARRIER LOCATION 4

Barrier location 4 is the alternative with the greatest depth of al the considered locations, which is approximately 81 m. Despite this fact, barrier location 4 still has the smallest 'to be closed' area (around 200000 m^2). This is due the small span of this location, approximately 7 km, making it the location variant with the smallest barrier span. Since the bathymetry of this location has a part of approximately 4 km that is relatively shallow, it makes this part very suitable for moveable barriers constructions. Also this barrier location provides protection to both Tokyo and Yokohama. But in difference to barrier location 2 and 3, this location provides also protection to Yokosuka, which is a city close to the mouth of the bay area. The subsoil of this location contains mainly sand and a small part of mud in the middle of the span. This the subsoil of this location relatively strong compared to the previous locations.

Advantage

- Shortest span (6.9 km)
- Smallest 'to be closed' area (around 200000 m^2)
- Protection Yokohama and Yokosuka
- Relatively strong subsoil
- Relatively shallow part (approximately 4 km) that is suitable for moveable barrier constructions

Disadvantage

- Barrier location with the greatest depth of all the considered locations (81 m)

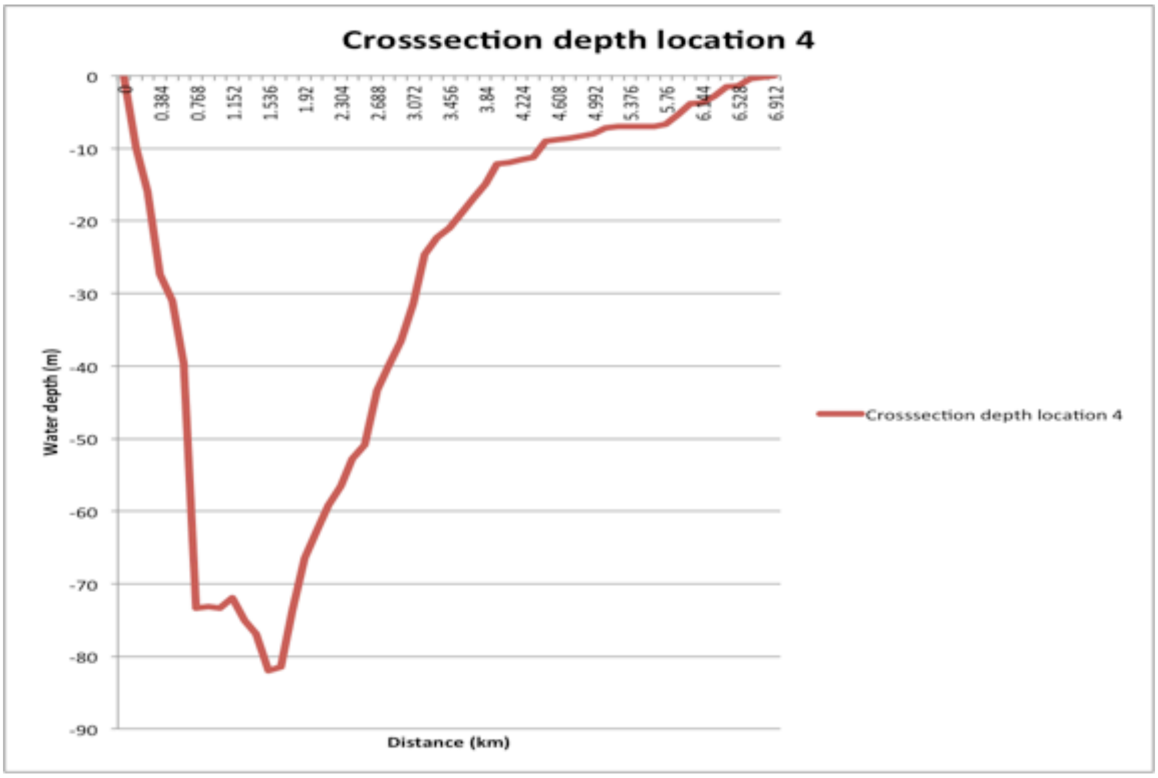

FIGURE 32: BATHYMETRY BARRIER LOCATION 4

5.1.5 BARRIER LOCATION 5

Just like barrier location 2 and 3, barrier location 5 is considered to compare the suitability of both bathymetries to build the barrier. Also this location takes both Yokohama and Yokosuka under it's protected area. The deepest part of this location is around 74 m, making it a bit less deep than barrier location 4. Also this location contains a relatively shallow part that is suitable for moveable barrier constructions. But due to it's long span (around 9.5 km) and large depth, this location alternative has a 'to be closed' area of around 300000 m², making it almost as big as barrier location 1. Also this location is really close to the mouth of the bay and faced to the mouth of the bay, which is also the direction of the waves coming from the sea (both typhoon and tsunami waves). This will probably make a barrier at this location suffer a greater wave load compared to the other locations. The subsoil of this barrier location contains mainly rock and sand.

Advantage

- Protection Yokohama and Yokosuka
- Relatively shallow part (approximately 5 km) that is suitable for moveable barrier constructions
- Relatively strong subsoil

Disadvantage

- Large depth (74 m)
- Large 'to be closed' area, around 300000 m²
- Faced to the direction of the incoming waves from the sea, therefore probably suffer larger wave loads.

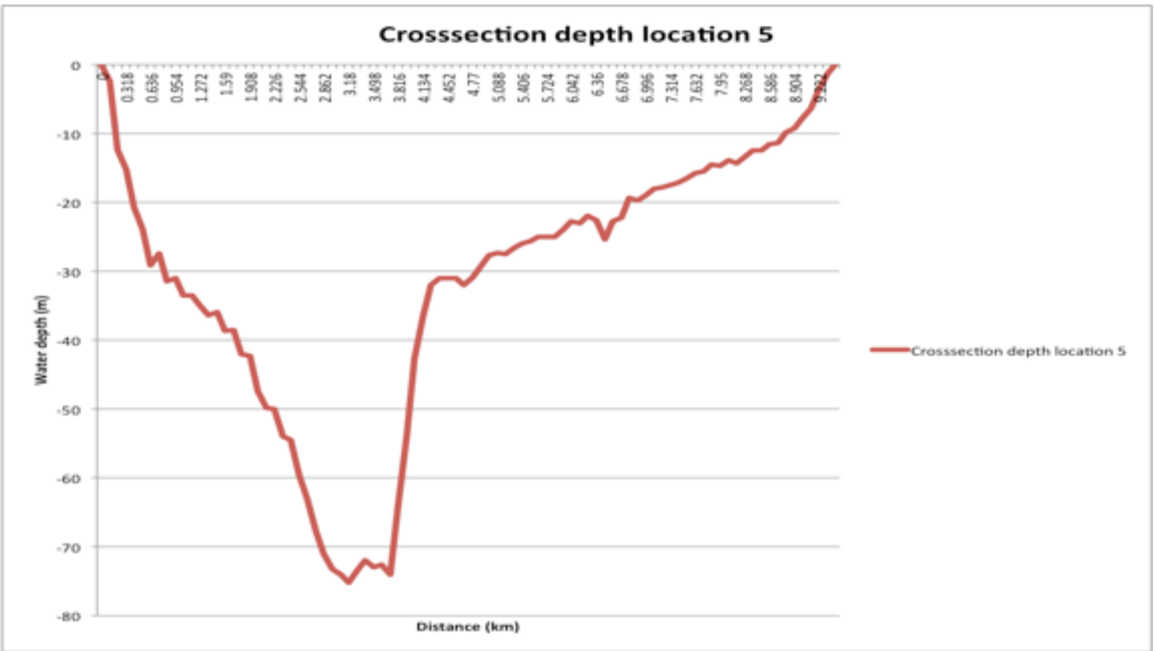

FIGURE 33: BATHYMETRY BARRIER LOCATION 5

6 APPENDIX 6: NAVIGATION CHANNEL DIMENSION CALCULATION

The minimum depth and width for the navigation opening in the barrier can be determined using the formulas developed by the PIANC group (Ligteringen, 2009). The dimensions of the chosen design ship Emma Marsk is given below:

D_s	[m]	Draft of design ship	= 15.5 m
W_s	[m]	Width of design ship	= 56 m
L_s	[m]	Length of design ship (LOA)	= 397 m

The minimum required channel depth is determined using the following formula (Ligteringen, 2009)

$$d_{nav} = D_s - \zeta_{tide} + s_{max} + \zeta_m + s_s = 17.25 \text{ m} = 17.5 \text{ m}$$

d_{nav}	[m]	Depth of navigation channel
D_s	[m]	Draft of design ship (= 15.5 m)
ζ_{tide}	[m]	Tidal elevation above reference level below which no entrance is allowed (= 0m)
s_{max}	[m]	Maximum sinkage due to squat and trim (= 0.75 m)
ζ_m	[m]	Vertical motion due to wave response (= 0.5 m)
s_s	[m]	Remaining safety margin or net under keel clearance (= 0.5 m)

The minimum width of the channel can be determined using a method developed by the PIANC group (Ligteringen, 2009). Since there is no information about the vessel speed, cross-winds and cross-current, they all assumed to be moderate.

It is chosen to have two-way navigation channels. The reason behind this choice is to anticipate the growth of the accepted ships in the future by the ports inside the bay.

The width of a two-way channel should fulfill the following requirement, the corresponding values are given in Table 11:

$$W_{min} = 2 * W_{BM} + \Sigma W_i + 2 * W_B + \Sigma W_p = 8.3 W_s = 464.8 \text{ m} = 465 \text{ m}$$

TABLE 11: VALUES OF REQUIRED WIDTH TWO-WAY CHANNEL

Width component	Condition	Width implication
Basic width W_{BM}	Good maneuverability	1.3 W_s
Additional width W_i		
Prevailing cross-winds	moderate	0.4 W_s
Prevailing cross-currents	moderate	0.7 W_s
Prevailing wave height	<1m	0.0
Aids to navigation	good	0.1 W_s
Bottom surface	<1.5D_s and rough/hard	0.2 W_s
Depth waterway	<1.25D_s	0.2 W_s
Cargo hazard	High	1 W_s
Bank clearance W_B	Steep and hard structures	0.5 W_s
Width for passing distance		
Vessel speed	moderate	1.6 W_s
Encounter traffic density	heavy	0.5 W_s

7 APPENDIX 7: TRAFFIC INTENSITY

This subsection calculates whether it is possible to let all of the vessels passing through two one-way navigation channel.

As stated in section 4.1.2.2, a daily average of 384 vessels going through Tokyo Bay, this might increase in the future. Therefor it is chosen to design the navigation channel for a traffic intensity of 400 vessels per day. Making it 200 vessels per day in each direction.

Since not every ship passing the navigation channel will be of size of the design vessel. The design geometry for ships passing the channel is assumed to be 250x35x14 (LxWxD).

Assuming a 12 hr day of service, the average time duration that a vessel will pass channel will be $\frac{12*3600}{200} = 216$ seconds. The distance between the consecutive vessels will be calculated based on a formula for vessels in inland waterway (Groeneveld 2002):

$$\frac{v_{lim}}{\sqrt{g * d_{nav}}} = 0.78 * (1 - \frac{A_s}{A_c})^{2.25}$$

v_{lim}	[m/s]	Limit speed of design vessel
d_{nav}	[m]	Depth of navigation channel (= 17.5 m)
A_s	[m^2]	Wet surface of design vessel (D_s*W_s = 490 m^2)
A_c	[m^2]	Flow area of channel ($d_{nav} \cdot W_{min}$ = $8137.5.5 m^2$)
L_s	[m]	Length of design ship (250 m)

Filling in the equation gives v_{lim} of 8.89 m/s.

Assuming that vessels will be sailing at half their limit speed every vessel needs 216*0.5*8.89 ≈ 960 m of space. According to Groeneveld (2002) the minimum mutual distance (i.e. from the stern of the ship traveling in front and the bow of the ship traveling behind) is 1.45*L_s . This means that the total minimum required space for each vessel is 1.45*L_s + L_s ≈ 612.5 m . This is minimum required length is smaller than the available space for each vessel, so the navigation channels are sufficient to handle the traffic intensity through the Tokyo Bay.

8 APPENDIX 8: TYPHOON

Typhoons are mostly located between latitudes of 30°S and 30°N and are low pressure systems that develop over the warm ocean waters. The rotation of typhoon is couter clockwise in the northern hemisphere and clockwise in the southern hemisphere. The formation of a tropical typhoon requires six conditions:

- Warm ocean waters of at least 26.5°C to a depth of minimal 50 m.
- An atmosphere that cools rapidly vertically transforming stored heat energy from the water into thunderstorm activity that fuels the tropical system
- Moist layers at mid troposphere elevations (5 kilometres altitude)
- Significant Coriolis forces to rotate the cyclone
- Presence of a near surface organized rotating system with spin and low-level inflow
- Minimal vertical wind shear at varying altitudes that can slice apart the cloud mass

Since the generation of the typhoon depends on warm ocean water, therefore it only appears in the midsection of the planet and it cannot be generated within 500 klimeters of the equator. The circulation of the thunderstorms is spinned by the pole-seeking centrifugal Coriolis force. In Figure 34 an overview of the anatomy of a northern

hemisphere hurricane is given.

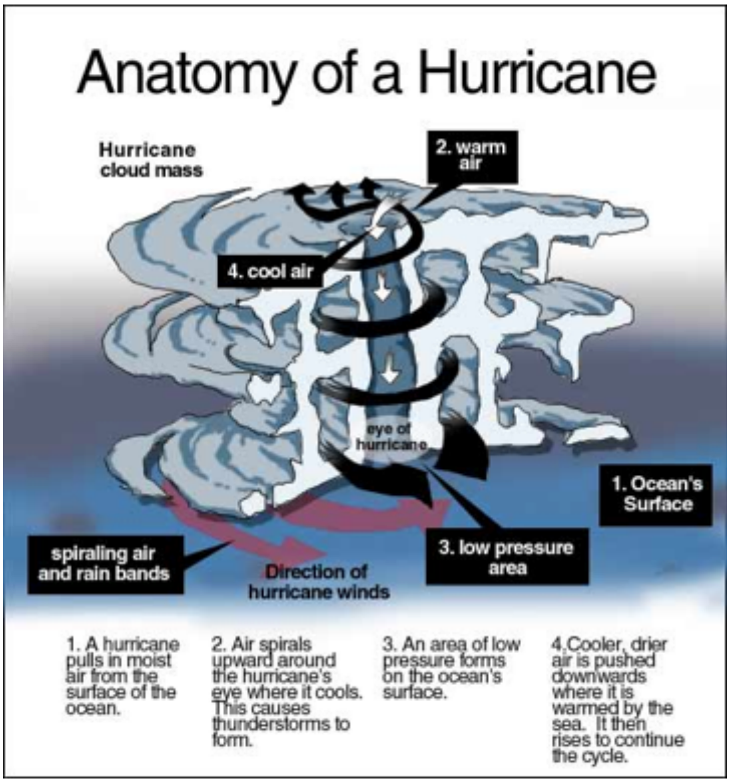

FIGURE 34: OVERVIEW ANATOMY NORTHERN HEMISPHERE HURRICANE

8.1 Different scales to classify hurricanes and typhoons

For the categorization of hurricanes and typhoons, several scales are used based on a combination of the hurricane characteristics of pressure, wind speed, storm surge and structural damage. For the Atlantic and Northeast Pacific basin, the Saffir-Simpson scale is used. It contains the destructive potential of hurricanes. While in Japan a scale of the Japan Meteorological Agency is used to classify typhoons. See Table 12 and Table 13.

TABLE 12: SAFFIR-SIMPSON SCALE TO SPECIFY HURRICANS

Cat.	Maximum Sustained Wind (1-min mean)		Effects
	[kt]	[km/h]	
One	64-82	118-152	No real damage to building structures. Damage primarily to unanchored mobile homes, shrubbery, and trees. Also, some coastal road flooding and minor pier damage
Two	83-95	153-176	Some roofing material, door, and window damage to buildings. Considerable damage to vegetation, mobile homes, and piers. Coastal and low-lying escape routes flood 2-4 hours before arrival of centre. Small craft in unprotected anchorages break moorings.
Three	96-113	177-208	Some structural damage to small residences and utility buildings with a minor amount of curtain wall failures. Mobile homes are destroyed. Flooding near the coast destroys smaller structures with larger structures damaged by floating debris. Terrain continuously lower than 5 feet ASL may be flooded inland 8 miles or more.
Four	114-135	209-248	More extensive curtain wall failures with some complete roof structure failure on small residences. Major erosion of beach. Major damage to lower floors of structures near the shore. Terrain lower than 10 feet ASL may be flooded requiring massive evacuation of residential areas inland as far as 6 miles.
Five	135	>248	Complete roof failure on many residences and industrial buildings. Some complete building failures with small utility buildings blown over or away. Major damage to lower floors of all structures located less than 15 feet ASL and within 500 yards of the shoreline. Massive evacuation of residential areas on low ground within 5 to 10 miles of the shoreline may be required.

TABLE 13: TYPHOON SCALE ACCORDING TO THE JAPAN METEOROLOGICAL AGENCY

JMA Category	Maximum Sustained Wind (10-min mean)		International Category	Class
	[kt]	[km/h]		
Tropical Depression	- 33	- 62	Tropical Depression (TD)	2
Typhoon	34 - 47	63 - 88	Tropical Storm (TS)	3
	48 - 63	89 - 118	Severe Tropical Storm (STS)	4
Strong Typhoon	64 - 84	119 - 156	Typhoon (TY) or Hurricane	5
Very Strong Typhoon	85 - 104	157 - 192		
Extreme Typhoon	105 -	193 -		

Beaufort scale (for wind speed) ends with category 12, with maximum sustained wind speeds above 117 km/h. That is equal the lowest category on the Saffir-Simpson scale. See Table 14.

TABLE 14: BEAUFORT SCALE

Cat.	Winds [km/h]		Effects
0	0-2	Calm	Land- Smoke rises vertically Water- Like a mirror
1	2-6	Light Air	L- Rising smoke drifts W- Small ripples
2	7-11	Light Breeze	L- Leaves rustle W- Small wavelets, wind fills sail
3	12-19	Gentle Breeze	L- Light flags extend W- Large wavelets, sailboats heel
4	20-30	Moderate Breeze	L- Moves thin branches W- Working breeze, sailboats at hull speed
5	31-39	Fresh Breeze	L- Small trees sway W- Numerous whitecaps, time to shorten sails
6	40-50	Strong Breeze	L- Large tree branches move W- Whitecaps everywhere, sailboats head ashore, large waves
7	51-61	Moderate Gale	L- Large trees begin to sway W- Much bigger waves, some foam, sailboats at harbour
8	62-74	Fresh Gale	L- Small branches are broken from trees W- Foam in well marked streaks, larger waves, edges of crests break off
9	75-87	Strong Gale	L- Slight damage occurs to buildings W- High waves, dense spray, visibility affected
10	88-102	Whole Gale	L- Large trees uprooted, considerable building damage W- Very high waves, heavy sea roll, surface white with spray and foam, visibility impaired
11	103-117	Storm	L- Extensive widespread damage W- Exceptionally high waves, small to medium ships obscured, visibility poor
12	117+	Hurricane	L- Extreme destruction W- Waves 40+', air filled with foam and spray, visibility restricted

8.2 Typhoon track over bays

The occurrence of flooding during a typhoon is highly influenced by its track. In the northern hemisphere, the highest wind speeds are located to the right (east) of the typhoon center. The higher winds to the right of the typhoon center originate from the summation of the round wind speed profile and the forward movement of the typhoon, see Figure 35. The Tokyo Bay is north-south oriented. If a typhoon center passes to the west of the bay, the maximum wind of the typhoon will affect the bay precisely. Together with the large fetch length, large storm surges will occur at the north end of the bay. See Figure 36. For bays that are east-west oriented due to the smaller wind speed in the direction of the bay axis and the smaller fetch in the direction of the maximum wind speed of the typhoon.

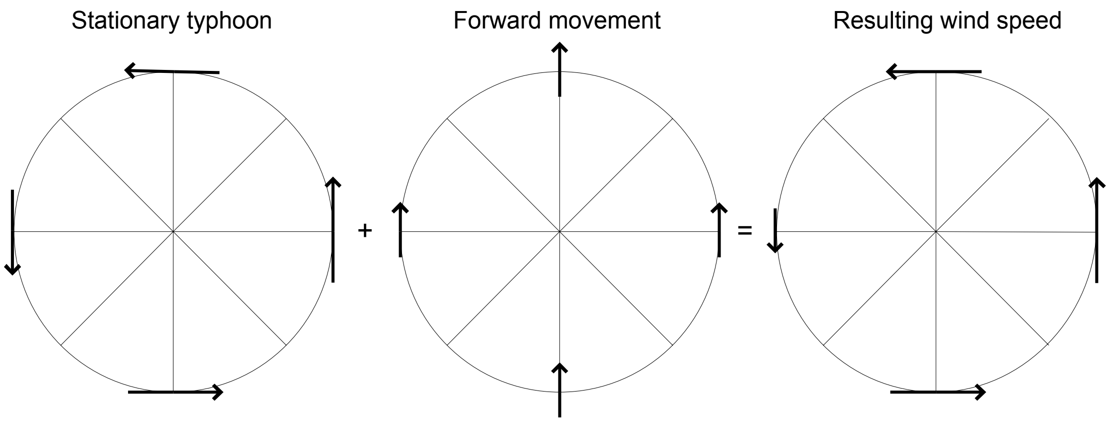

FIGURE 35: RESULTING WIND SPEED TYPHOON DUET O FORWARD MOVEMENT (NORTHERN HEMISPHERE)

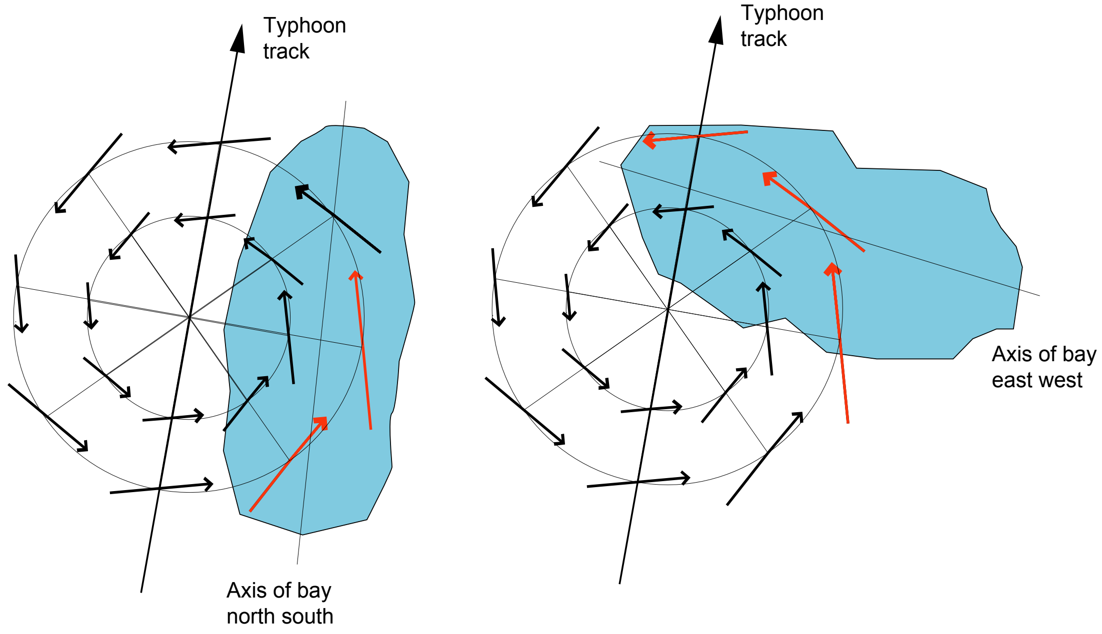

FIGURE 36: DIFFERENT ORIENTATIONS OF BAY-AXES RELATIVE TO THE TYPHOON TRACK

8.3 Parameters that are used to describe a typhoon field

In generally typhoon wind fields can be represented by three parameters.

- The minimal atmospheric pressure of the typhoon center indicates the intensity of the storm. In Figure 37 a pressure distribution for an average typhoon is shown.
- The speed of the forward movement.
- The radius to maximum wind speed of the typhoon, which describes the size of the typhoon field. In Figure 38 a wind field of a typhoon with a radius to maximum wind speed of 84 km is shown.

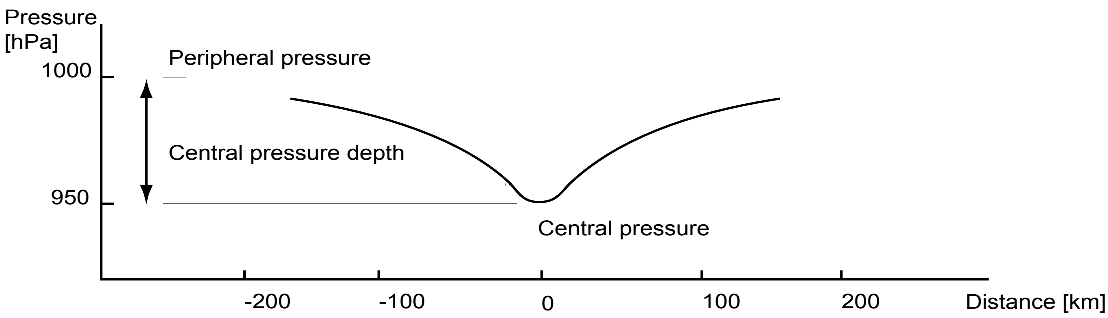

FIGURE 37: PRESSURE DISTRIBUTION FOR AN AVERAGE TYPHOON (CENTRAL PRESSURE DEPTH: 50 HPA)

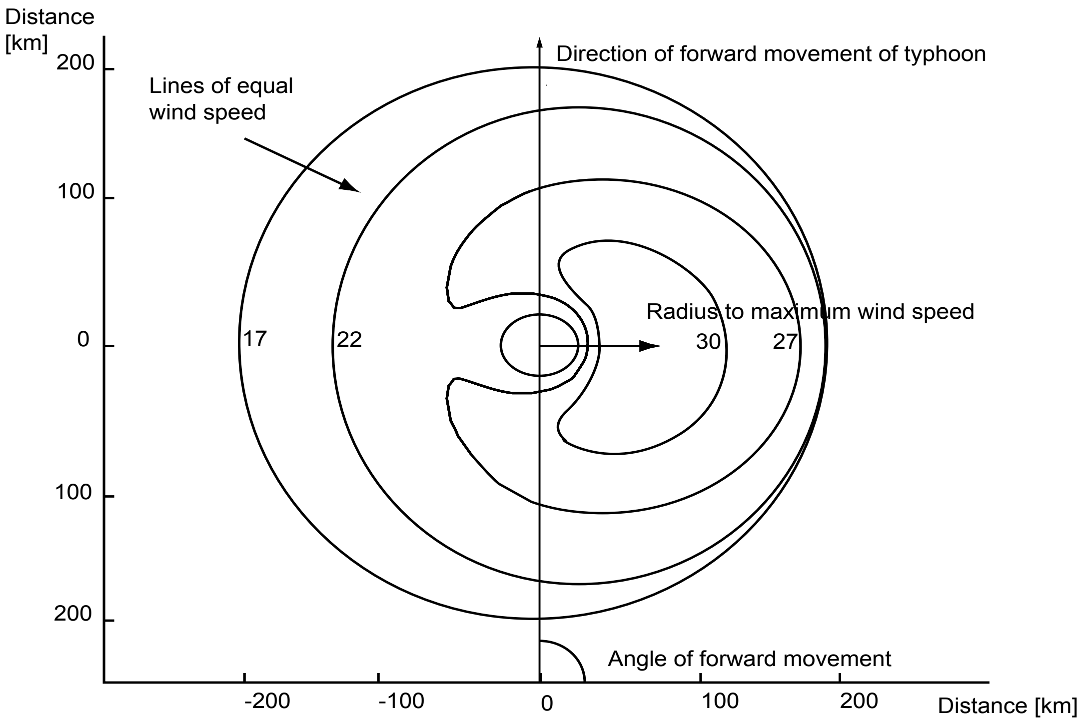

FIGURE 38: MAGNITUDE OF WIND FIELD (RADIUS TO MAXIMUM WIND SPEED: 84 KM) AND ANGLE OF FORWARD MOVEMENT RELATIVE TO A CERTAIN FIXED DIRACTION (EXAMPLE: 90 DEGREES); WIND SPEEDS IN M/S

8.4 Typhoon related storm surges

When the typhoon center passes the water on its west side (northern hemisphere), large storm surges may occur due to the large wind speed on the right side of the typhoon. The storm surge height is influenced by the local pressure and the wind stress on water caused by the local winds. These are again related to the storm speed, direction of approach, bottom topography, and coincidence with high tide level. A storm surge is generated by three different phenomena:

- The suction effect of the decrease in atmospheric pressure or pressure set-up
- The wind drift effect or wind set-up
- Static wave effects caused by wave breaking or wave set-up

8.4.1 PRESSURE SET-UP

The low pressure in the eye of a typhoon results in an increase in water level that is concentrated in the center of the typhoon. This phenomenon is known as the Inverse Barometer Rise effect or pressure set-up. A rule of thumb is that with every hectopascal decrease of atmospheric pressure, the water level rises with one centimeter.

8.4.2 WIND SET-UP

When the typhoon wind blows over the water surface, it increases the mean water level due to the piling up of water on the shore. This process is caused by the friction of the wind over the water surface and results in inclination of the water level in situations with limited water depths. The wind set-up is not only dependent on the wind speed, but also on the fetch length and the water depth.

8.4.3 WAVE SET-UP

Wave set-up is the increase of mean water level due to the presence of waves. As a progressive wave approaches shore and the water depth decreases, the wave height increases due to wave shoaling, which will eventually cause wave breaking. After the waves break, the energy dissipation causes the radiation stress to decrease, which will result in the increase of free surface level to balance it: wave set-up. The wave set-up can reach about ten percent of the offshore wave height. This phenomenon is specifically for beaches with mild bed slope

9 APPENDIX 9: GEOLOGICAL BOUNDARY CONDITION

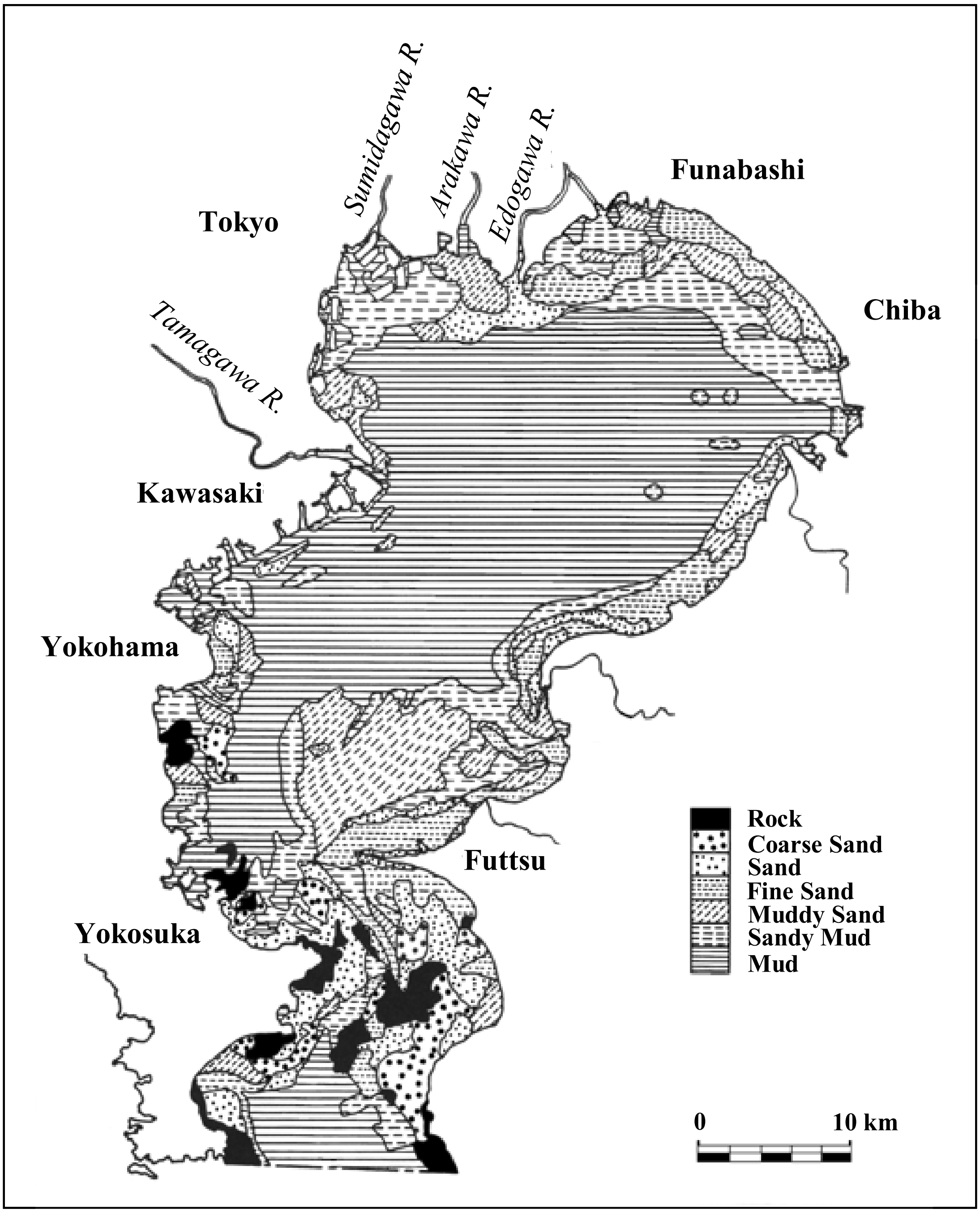

10 APPENDIX 10: WATER LEVEL RISE INSIDE THE BAY WITH PERMANENT OPEN NAVIGATION CHANNEL

For this calculation the 'rigid-column approximation' (Labeur, 2007) will be used. The schematic view of the model is given in Figure 39. It is assumed that during storm surge the non-navigation parts of the barrier are fully retaining. The formula of this approximation is given below.

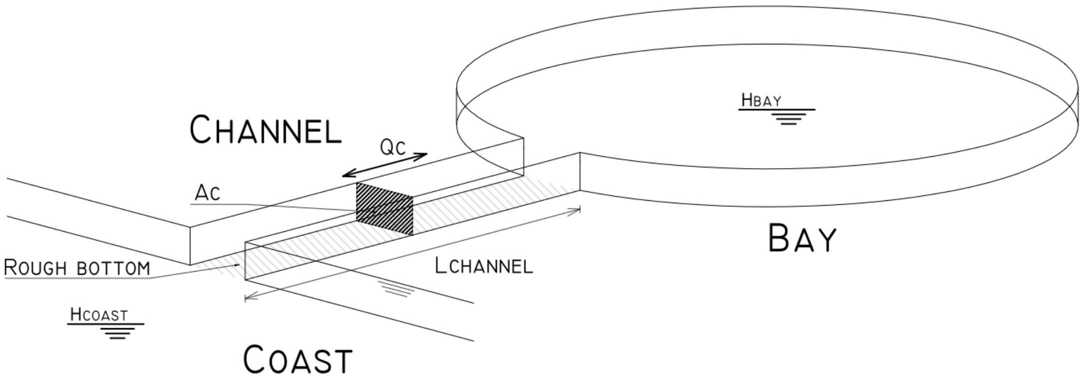

FIGURE 39: SCHEMATIC VIEW OF THE RIGID COLUMN APPROXIMATION (VRIES, 2014)

$$\zeta_{bay} = r * \zeta_{sea}$$

$$r = \frac{1}{\sqrt{2} * \Gamma} * \sqrt{\sqrt{1 + 4 * \Gamma^2} - 1}$$

$$\Gamma = \frac{8}{3 * \pi} * \chi * (\frac{A_k}{A_s})^2 * \frac{\omega^2}{g} * \zeta_{sea}$$

Where:

ζ_{bay} = Water level rise inside the protected area.
ζ_{sea} = Water level rise sea during storm surge.
r = Amplitude ratio
Γ = Measure for relative magnitude of the resistance.
χ = Loss factor (0.5 for closing gap bay)
A_k = Protected area (920 km^2)
A_s = Flow area navigation channel (465 x 17.5 = 8137.5 m^2)
ω = Angular velocity storm surge
g = Gravitational acceleration

It is assumed that the moveable barriers will be closed off at the moment when the water level inside the bay is at its lowest point. Since in this stage of the design it is not clear how many moveable barriers are going to be placed, the water level inside the bay will be checked assuming a permanently closed storm surge barrier with a permanently open navigation channel. Note that this assumption gives a much smaller allowable water level rise inside the bay compared to the actual situation with the moveable barrier due to the smaller tidal inlet and the wind set-down in neglected in this design stage.

The corresponding tide has a maximum tide level of 0.966 m. Since it is a semidiurnal tide, the duration of the tide is assumed to be 6 hours. The corresponding angular velocity of the tide sequence is then:

$$\omega = \frac{2\pi}{T} = \frac{2\pi}{12 * 3600} = 0.0001454\, rad/s$$

By filling in the formula, it results in an amplitude ratio of 0.5 and a 0.48 m tidal inlet. The minimum water level inside the bay is reached 0.6 hour before the start of the assumed typhoon condition. Since during this calculation the storm surge barrier is assumed to be fully closed off except for the navigation channel, the water level inside the bay at the start of the typhoon is the same as the water level at the end of the tidal cycle. See

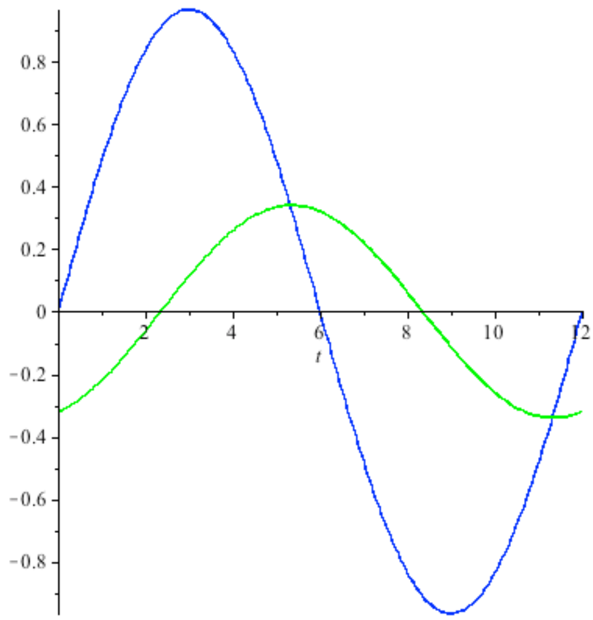

FIGURE 40: COMPARISON TIDAL LEVEL SEA SIDE (BLUE) WITH WATER LEVEL RISE INSIDE THE BAY (GREEN) WITH PERMANENT OPEN NAVIGATION CHANNEL, VERTICAL AXIS: WATER LEVEL RISE IN M, HORIZONTAL AXIS: TIME IN HOURS.

From this graph it can be seen that the water level inside the bay right before the assumed typhoon condition is 0.32 m under the mean water level inside the bay.

The total water level rise inside the protected area by year 2100 also includes the following aspects.

- Pressure set-up (1.12 m)
- Wind set-up Tokyo (0.72 m)
- Sea level rise 2100 (1 m)
- River discharge (0.004 m)
- Wave overtopping (neglected in this stage)

The maximum allowed water level rise in the protected area caused by the flow through the permanent open navigation channel is then:

$$3.466 - 1.12 - 1 - 0.72 - 0.004 - 0.5 + 0.32 = 0.44\,m$$

Note there is a 0.5 m freeboard taken into account.

The duration of the typhoon is also assumed to be 6 hours; this can be seen as half of the fictional storm surge wave. Therefor the period two times the duration of the typhoon, which is 12 hours. This results in the same angular velocity as the tides.

Since the pressure set-up just inside and just outside the protected area is approximately the same, the maximum water head at the barrier during the typhoon is given in the equation below. Note that since this an initial estimation of the water level rise, the effect of wind set-down at the barrier is being neglected.

$$tide + wind\ set\ up + 0.32 = 0.966 + 0.16 + 0.32 = 1.44\,m$$

By filling in the formula, it results in an amplitude ratio of 0.29 and a 0.41 m water level rise of the protected area inside the bay.

The water level rise caused by the open navigation channel is below the maximal allowed water level rise. Therefor it is possible to keep the navigation channel permanent open during the design storm surge. The development of the assumed storm surge plus tide together with the corresponding water level rise inside the bay is plotted against time, see Figure 41. Note in reality that the second part of the storm surge wave in the graph (after 6 hours) has a much smaller amplitude since it only contains the tide.

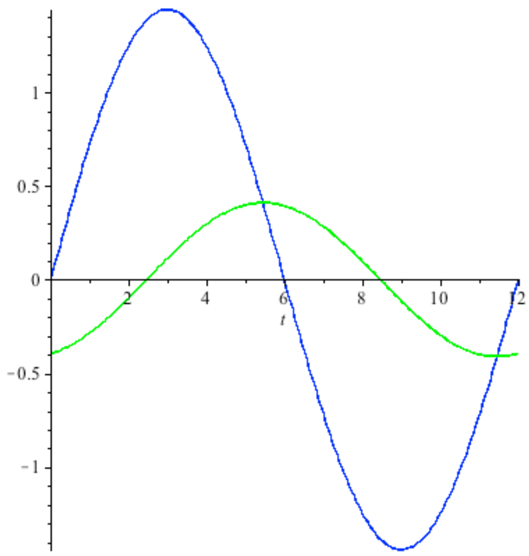

FIGURE 41: WATER LEVEL RISE STORM STORM SURGE (BLUE) COMPARISON WITH WATER LEVEL RISE INSIDE THE BAY (GREEN) WITH PERMANENT OPEN NAVIGATION CHANNEL, VERTICAL AXIS: WATER LEVEL RISE IN M, HORIZONTAL AXIS: TIME IN HOURS.

11 APPENDIX 11: GRAVITY BASED FOUNDATION

Gravity based foundation, or GBF, is a shallow foundation technic that is often used in the offshore industry. As the name already indicates, this type of foundation uses weight to maintain and support the upper structure. This is often done using big heavy concrete under structures.

Due to its great size and weight, it is really difficult to make it on site. Therefor a GBF is often prefabricated and transported to site afterward. The transportation can be done in different ways; it depends on the size and weight of the foundation structure which transportation method is used. Smaller GBF's till a weight of 14200 ton can often be transported using floating cranes and pontoons. Bigger GBF's are build in such a way that it can float by itself and are dragged to the construction site by barges. Before the GBF can be installed to the sea bottom, the subsoil of the corresponding construction site has to be prepared for the installation. During the preparation of the subsoil, first the soft silt at the top of the subsoil will be removed till a part that is strong enough to retain the weight of the GBF and the upper structure. Note that if this strong part is too deep, soil improvements of soil replacement are then needed. After putting a layer gravel on top of the excavation, the GBF can be submerged into the excavation using cranes or ballast. When the GBF is successfully submerged, it will be pumped full with sand in order to create the 'gravity', which is responsible for the stability of the foundation. The excavation will then filled up with sand to the original sea bottom level. This process will give the GBF even more stability by mooring it into the ground. In order to prevent erosion at the filled up sand layer, bottom protection will be applied on top of the filled up layer.

12 APPENDIX 12: PILE FOUNDATION

Pile foundation is a deep foundations are foundations that are embedded deep into the ground. The main reason to choose a deep foundation over a shallow foundation is because of the large design load of the upper structure and poor soil quality at shallow depth. Piles are generally driven into the ground in situ, but it can also be put in place using drilling. The material used for the pile can vary from timber, steel, reinforced concrete and prestressed concrete.

12.1 Driven piles

Driven piles are prefabricated piled that are driven into the ground using a pile driver. With respect to drilled piles, the advantage of driven pile is because the soil displaced by pile driving compresses the surrounding soil. This phenomenon will increase the loadbearing capacity of the pile by causing greater friction against the sides of the piles.
Foundations relying on driven piles are often connected to groups using a pile cap, which is a large concrete block where the heads of the piles are embedded. The reason to use this method is to distribute the loads that are large that the load one pile can bear. These pile caps or isolated piles are typically connected using grade beams; lighter structural elements of the upper structure can bear on these grade beams, while heavier elements bear directly on the pile cap.

12.2 Drilled piles

Drilled piles are casted in-situ. By using rotary boring technique, this pile foundation method permits pile construction through particularly dense or hard soil layers. The drilling method of the piles depends on the geology of the site. Both the diameter and depth of the piles are high specific to the ground conditions, loading conditions and the nature of the upper structure. For end-bearing piles, drilling continues until the borehole has reached a sufficient depth into a sufficient strong soil layer.

13 APPENDIX 13: ALTERNATIVE GATES FOR THE OPENING

In this chapter, different types of gates for the storm surge barrier are compared in order to find the right solution for the problem. Also different reference projects of the considered types of gates will be described. For every reference project the cost/m barrier will be given. Note that this estimation doesn't consider the depth of the bathymetrie and the precise distribution of gates, so the compared price will deviate from the actual price. Also the cost for most of these barriers are including maintenance cost untill now. Despite this, the price will give an qualitative indication of the barriers cost.

13.1 Flap gate

Floating bottom flap gates are gates that are connected to the bottom of the water with a hinge. In opened position it is resting on the water bottom. The gate is then filled with water. When closing, air will be pumped in the gate and water will be pumped out so the gate will float. See Figure 42 for a principle sketch. The flap gates are very favorable for conditions with long gate span. This type of gate can be build in separate elements with smaller span, so theoretically an unlimited gate length can be accomplished with this type of gate

Since the gate in stored under water in the open state, there is no visual hindrance under normal condition. This is also the main reason for the application of the flap gate in the MOSE project in Venice. The biggest disadvantage of the flap gate is its costs. Also the maintenance of it is difficult since a large part of the gate is under water.

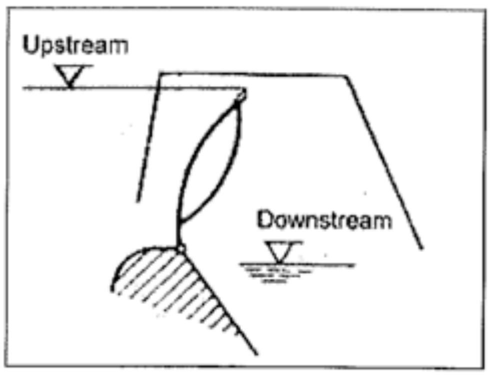

FIGURE 42: PRINCIPLE SKETCH BOTTOM FLAP GATE

Advantage:

- Unlimited vertical clearance in opened position for navigation.
- No visual obstacle in opened position.
- Advantage in neutralizing wave impact due to its flexibility
- Long span with separated elements

Disadvantage:

- Difficult maintenance
- Expensive

13.1.1 REFERENCE PROJECT: VENICE BARRIER

<u>Description</u>
The number of flooding of Venice has increased in the last couple of years. Therefor it is decided to close of the lagoon of Venice with a barrier when the tide is higher than 110 cm. the barrier is a part of the MOSE-system: three lagoon entrances can be close off by bottom flap gates. Under normal circumstances, the bottom flap gates will be filled with water and rests in the sill at the bottom of the entrance. During higher water, the gate will be filled with air and the water will be pumped out. Hereby the gates will float up. The gates will oscillate due to the varying water level.

Scale:
Total number of gates: 78
Average gate width: 20 m
Maximum dimension of one gate: 20 m wide, 29.6 m high, 5 m thick

<u>Cost</u>:
Total cost: 5.3 billion euro (not completely finished yet)
Cost/m: 3.4 million/m

FIGURE 43: VENICE BARRIER GATES FLOATED UP

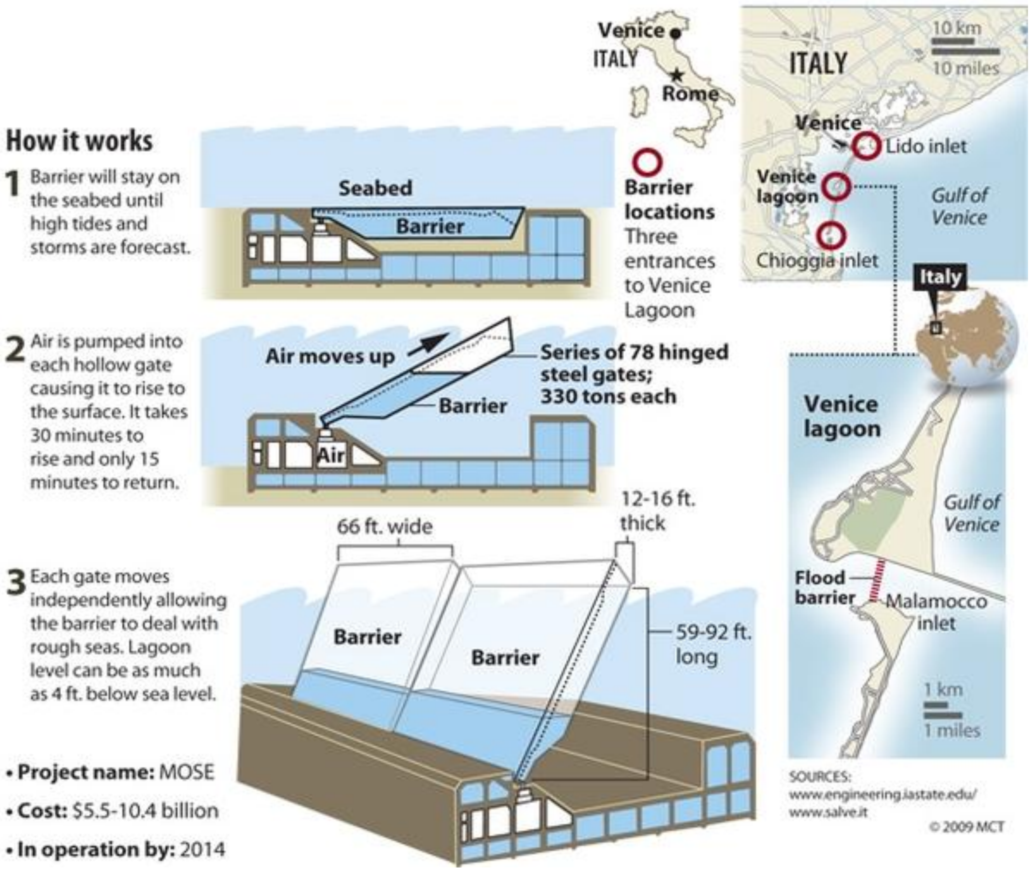

FIGURE 44: VENICE BARRIER WORKING PRINCIPLES

13.2 Radial gate

This type of gate rotates around a rotation point using a mechanical driven system. In opened position, the gate above the water surface and will be lowered when it needs to be closed. See Figure 45 for a principle sketch. Radial gate is a cheap, simple and reliable gate type for many applications. It is one of the most used moveable water control structure as they are applied in many dams. The biggest disadvantage of this barrier type is its limited vertical clearance for navigation and visual hindrance.

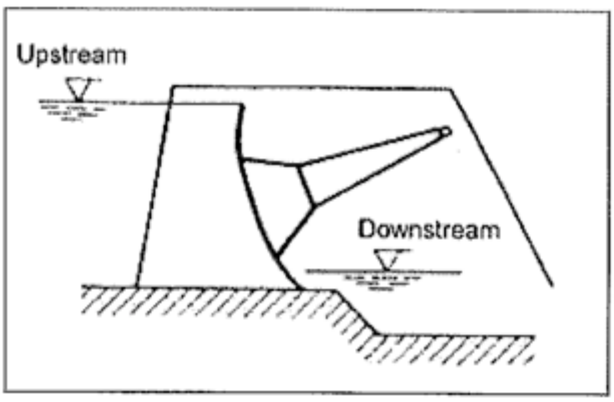

FIGURE 45: PRINCIPLE SKETCH ROTATING SEGMENT GATE

Advantage:
- Maintenance can be performed above water

Disadvantage:
- High concentration compressive stress at the rotation points.
- Limited vertical clearance for navigation.
- Visual disturbance in opened position.

13.2.1 REFERENCE PROJECT: EMSSPERWERK

Description
The Ems is a river in Germany that debouches in the Dollart. The Emsperrwerk serves both as a storm surge barrier and as a weir in order to make navigation that requires bigger depth possible. The barrier is build between 1997 and 2002 and locates 4 km upstream of Dollart. It consists 5 lifting gates, 1 cylinder gate for the sea navigation and 1 rotating segment gate for the inland navigation. The cylinder gate can be rolled down to the water bottom, which leads to unlimited vertical clearance for the navigation.

Scale
Total length: 476 m
Rotating segment gate: 60 m wide, -9 m sill height

Cost:
Total cost: 380 million euro (2010)
Cost/m: 0.8 million/m

FIGURE 46: EMSSPERRWERK TOP VIEW

FIGURE 47: EMSSPERRWERP WITH UNLIMITED VERTICAL CLEARANCE

13.3 Vertical lifting gate

A relatively often-used type gate. In opened position, the gate hangs at a certain height above the water surface and will be lowered when it needs to be closed. See Figure 48 and Figure 49 for principle sketches. Much experience and knowledge is available for its construction and behaviors under flow and wave conditions. The span of these gates can be up to 100 m and the maintenance is relatively simple. The biggest disadvantage of this barrier type is its limited vertical clearance for navigation and its visual hindrance.

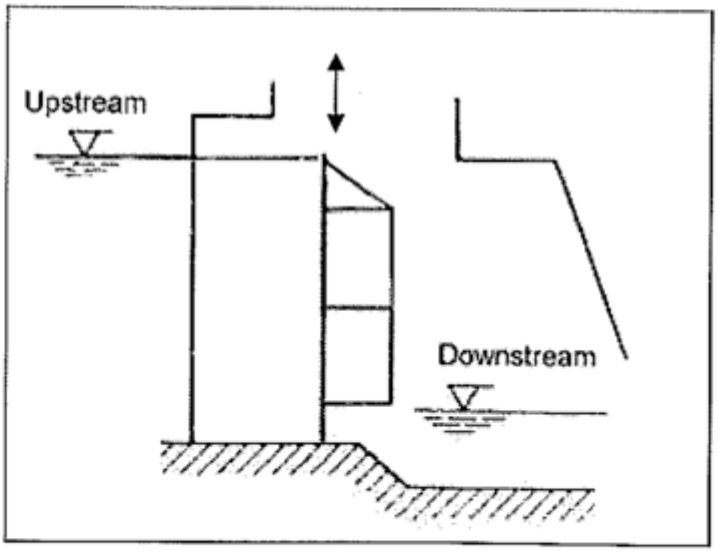

FIGURE 48: PRINCIPLE SKETCH LIFTING GATE SIDE VIEW

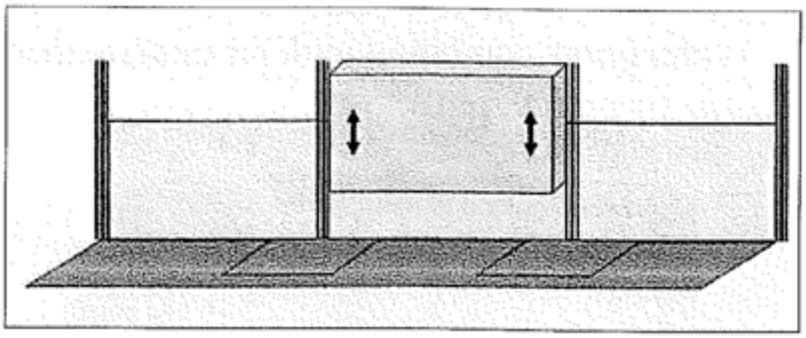

FIGURE 49: PRINCIPLE SKETCH LIFTING GATE FRONT VIEW

Advantage:

- Commonly used solution, lots of experience in building this.
- Maintenance can be performed above water.

Disadvantage:

- Limited vertical clearance for navigation.
- Visual disturbance in opened position.
- Large mechanic driven system needed to lift the gate, especially with long span.

13.3.1 EASTERN SCHELDT BARRIER

Description

The Eastern Scheldt is a estuaries in the Netherlands that lies in the north of the Western Scheldt. It contains a great variation of fish and water plants. According to the first Delta plan f the Netherlands, the Eastern Scheldt needed to be closed completely in order to increase safety. But this decision has led to large discussions, primarily about nature conservation and the impact of the fishery in that region. Therefor it is in 1975 decided to construct a open storm surge barrier that can be closed during high water level.

The barrier consists of bottom protection, concrete columns with steel lifting gates in between. A sash lock was constructed for the purpose of navigation. The bottom of the lock lies 7 m under NAP. The governing ship size for the lock is 200 x 23 x 4.75 m.

Scale

Total length: 2800 m
3 trenches and 62 steel lifting gates.

Cost

Total cost: 2.5 billion euro (1986)
Cost/m: 0.9 million/m

FIGURE 50: EASTERN SCHELDT BARRIER SIDE VIEW

FIGURE 51: EASTERN SCHELDT BARRIER TOP VIEW

13.4 Inflatable rubber gate

With this kind of gate, a. inflatable rubber bellow is attached to the structure at the bottom of the water. In closed position, the bellow is empty and rests in the bottom structure. When the gate needs to be closed, water and air will be pumped into the bellow to inflate the bellow. See Figure 52 for principle sketch. The rubber bellow can be fixed to the bottom structure using clamp plates and anchor bolts. Just like the flap gate, the biggest advantage of this barrier its applicability for long spans as it can be separated into smaller elements and its low investment cost. The biggest disadvantage of this barrier type is its sensitivity to external damage from floating objects like ships and debris, leading to higher chance for high maintenance cost.

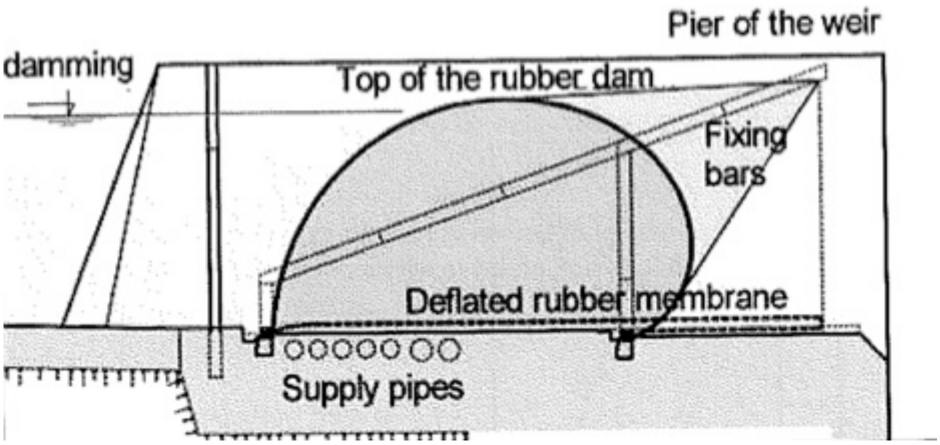

FIGURE 52: PRINCIPLE SKETCH BELLOW BARRIER

Advantage:

- Unlimited vertical clearance in opened position for navigation.
- Little visual obstacle in opened position.
- Advantage in neutralizing wave impact due to its flexibility.
- Long span with separated elements

Disadvantage:

- The inflatable bellow is vulnerable for external damage.
- Maintenance has to be performed under water.

13.4.1 REFERENCE PROJECT: RAMSPOL BELLOWS BARRIER

Description

During high water at IJselmeer, the Ramspol bellows barrier can shut off the entrance of the Zwarte Meer. Hereby the area till Zwolle will be protected against flooding. During normal circumstances, the bellows barrier lies at the bottom of the Zwarte Meer. During high water, it will be filled with water and air in order to inflate the rubber membrane that will act as the barrier.

<u>Scale</u>:
The barrier consists of 3 bellows, each with a length of 80 m.
Bottom position: 4.65 m under NAP
Design height: 8.35 m.
Bellow width: 8 m

<u>Cost</u>:
Total cost: 136 million euro (2010)
Cost/m: 0.57 million/m

FIGURE 53: RAMSPOL BELLOWS BARRIER TOP VIEW

FIGURE 54: RAMSPOL BELLOWS BARRIER DURING STORM

13.5 Vertical rotating gate

The cylinder gate rotates around the rotation point on both sides. In opened position, the gate is rotated flat to the bottom, and when it needs to be closed, the gate will be rolled up. See Figure 55 and Figure 56 for principle sketches. The gate is supported on both side in hollow steel side disks that rotates in a vertical plane around central pivot bearings mounted on the piers. In order to counter balance the weight of the gate body, the side disks are partly filled with cast iron. By rotating the upwards outside the water, the gate can be easily accessed for maintenance. This is also the biggest advantage of this barrier type. The biggest disadvantage for this barrier type is its span limitation and large investment cost.

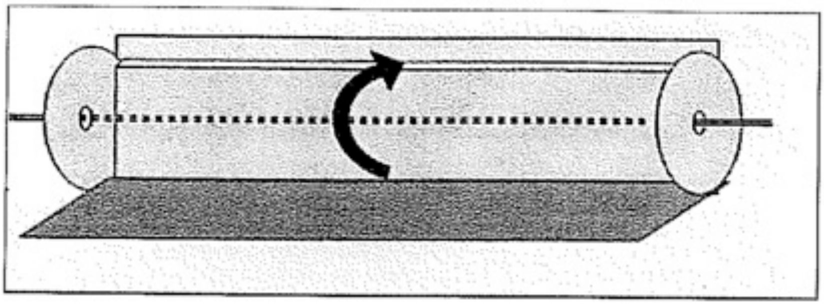

FIGURE 55: PRINCIPLE SKETCH CYLINDER GATE REAR VIEW

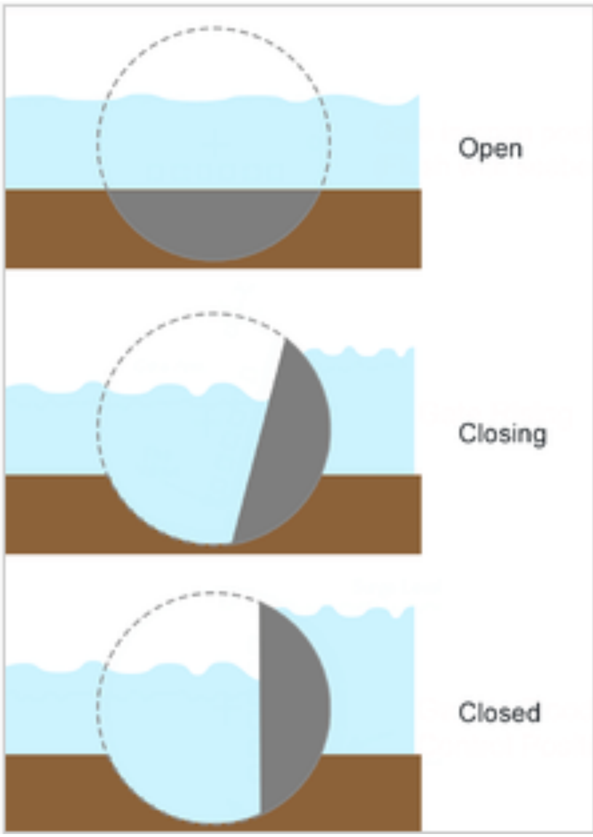

FIGURE 56: PRINCIPLE SKETCH CYLINDER GATE CROSS SECTION

Advantage:

- Unlimited vertical clearance in opened position for navigation.
- Little visual obstacle in opened position.
- Maintenance can be performed above water just by rolling up the gate.

Disadvantage:

- Concentrated stress at the rotation points.
- Expensive
- Limited span

13.5.1 REFERENCE PROJECT: THAMES BARRIER

Description

The Thames barrier protects London against high water from the North Sea since 1984. The width of the Thames river at the location of the barrier is 525 m. The barrier consists of 6 cylinder gates of 61 m wide, 2 cylinder gates of 41 m wide and 4 lifting gates. If the barrier is not in use (open), the arc-shaped gates lie on the water bottom. It will be rolled up by 90 degrees during high water in order to retain the water. Maintenance of the gates can be done relatively easy by simply roll up the gate above the water surface.

Scale

Total length: 525 m

Maximum door width: 61 m

Cost

Total cost: 1.5 billion euro (2010)

Cost/m: 2.86 million/m

FIGURE 57: THAMES BARRIER TOP VIEW

FIGURE 58: THAMES BARRIER CYLINDER GATE

FIGURE 59: THAMES BARRIER MAINTENANCE POSSIBLE BY ROLLING UP THE CYLINDER GATE

13.6 Sector gate

The horizontal sector gates rotate horizontally around a vertical axis on both sides. In the opened position it rests in the dry dock on banks on both sides of the waterway. See Figure 60 for principle sketch. Sector gates can be either floating or non-floating, but it is preferable to have floating sector gates. This is because the big disadvantage of non-floating sector gates needing deep side chambers in the abutment where the gates are housed when they are not in use. Also non-floating sector gates bears higher risk of malfunctioning when siltation occurs on the sill. The biggest disadvantage for sector gates is the concentrated force on the rotation points, making it a critical and vulnerable point.

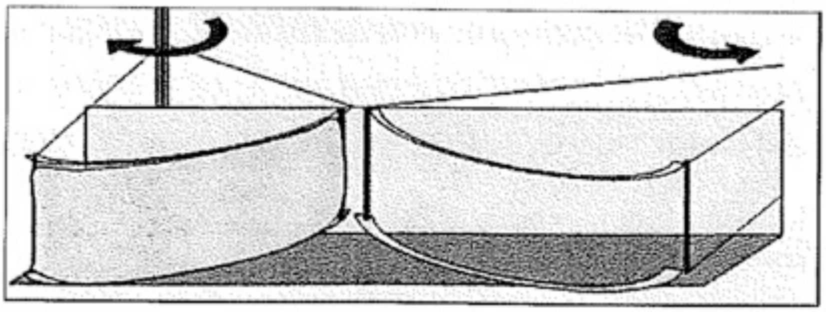

FIGURE 60: PRINCIPLE SKETCH HORIZONTAL SECTOR GATE FRONT VIEW

Advantage:

- Unlimited vertical clearance for navigation.
- Maintenance can be performed in the dry dock.

Disadvantage:

1. Concentrated forces on rotation points.
2. Needs extra space alongside the waterway.

13.6.1 REFERENCE PROJECT: MAESLANT BARRIER

Description

The Maeslant barrier is a storm surge barrier that can close off the Nieuwe Waterweg in the Netherlands during high water. The barrier consists of two horizontal sector gates. The gates are connected to the ball joint on the bank by a truss arm. When the barrier is open, the gates lie in the dock on the bank. It can be closed by first flooding the dock causing the gates to float and then close it by using the engine on the bank. When the floating gates meets each other in the Nieuwe Waterweg, the empty spaces inside the gate will be filled with water and the gate will sink to the bottom. It can be opened again just by pumping out the water again.

Scale:

Width Nieuwe Waterweg: 360 m

Depth: 17 m

Length truss arm: 237 m

<u>Cost:</u>

Total cost: 450 million euro (1997)

676 million euro (2010), inclusive dike strengthening and the Europoort barrier.

Maintenance and control: 5 million euro per year.

Cost/m: 1.9 million/m

FIGURE 61: MAESLANT BARRIER TOP VIEW

FIGURE 62: MAESLANT BARRIER IN DRY DOCK

13.6.2 REFERENCE PROJECT: IHNC LAKE BORGNE SURGE BARRIER

Description

In December 2008 New Orleans started the construction of the Inner Harbor Navigation Canal (IHNC) storm surge barrier. During a hurricane the barrier will close off the connection with the Gulf of Mexico. The total barrier has a length of approximately 3 km, consisting one retaining wall with two navigation openings with closeable gates. The gates of this barrier is comparable with the Maeslant barrier. Because of the weak subsoil in the area. It was decided to use concrete retaining walls instead of a conventional dike. On August 29, 2012 the barrier was closed for the first time to protect the city from hurricane Isaac.

Scale:

Total width: circa. 3000 m

Cost:

Construction cost: 815 million euro

Cost/m: 0.27 million/m. Note that the low price/m is due to the large part closure dam.

FIGURE 63: IHNC LAKE BORGNE SURGE BARRIER UNDER CONSTRUCTION

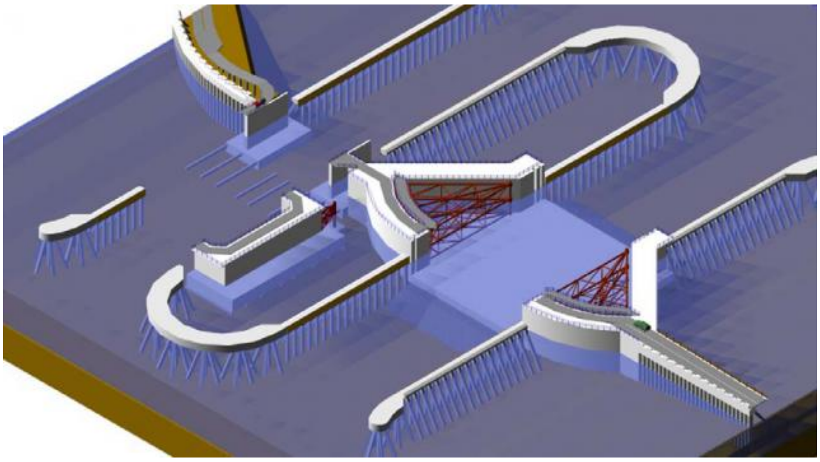

FIGURE 64: IHNC LAKE BORGNE SURGE BARRIER IMPRESSION DRAWING

13.7 Horizontal sliding gate

The horizontal sliding gates slides in or out the waterway during closing and opening of the gate. It can be one gate or two gates. See Figure 65 for principle sketch.

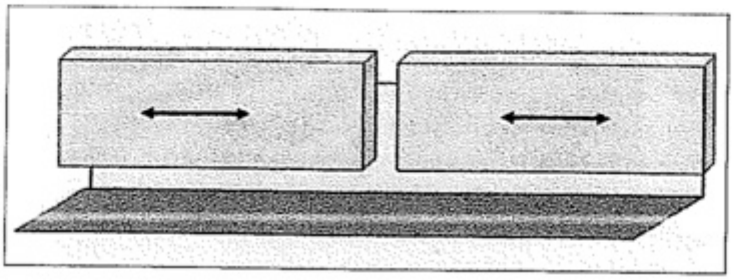

FIGURE 65: PRINCIPLE SKETCH HORIZONTAL SLIDING GATE (TWO GATES)

Advantage:

- Simple structure
- Unlimited vertical clearance for navigation.
- Maintenance can be performed in the dry dock.

Disadvantage:

- In case of two gates, great moment generated at the support of the gate because there is no support in the middle.
- Needs extra space alongside the waterway.

13.7.1 REFERENCE PROJECT: ST. PETERSBURG STORM SURGE BARRIER

Description
St. Petersburg is located on the Gulf of Finland near the mouth of the river Neva. in the history, the city has suffered flooding regularly from a high water level in the Gulf of Finland. Therefor in 1978, this barrier was designed in order to shut off the eastern part of the Gulf of Finland during high water. The barrier locates both to the north and south of the island Kotlin. Behind the barrier lies the ports of St. Petersburg and one marine port. Due to strategic reasons both the northern and the southern part of the barrier consists a storm surge barrier with unlimited vertical clearance. The storm surge barrier consists the following parts: 11 dams, 6 locks and two passage space for navigation. The northern channel can be closed off with a lifting gate. The southern channel can be closed using 2 horizontal sector gates, which are connected to the bank by truss arms.

Scale:
Total length barrier: 25.4 km
Dimension northern waterway: 110 m wide and 7 m depth
Dimension northern waterway: 200 m wide and 16 m depth

Cost:
More than 3.85 billion euro

FIGURE 66: ST. PETERSBURG STORM SURGE BARRIER NORTHERN GATE

FIGURE 67: ST. PETERSBURG STORM SURGE BARRIER SOUTHERN GATE

FIGURE 68: ST. PETERSBURG STORM SURGE BARRIER SEA LOCK

13.8 Visor gate

The Visor gate is arc-formed gate loaded under compressive force. In the opened position, it is rolled up, hanging above the water. The gate will be rolled down again when it needs to be closed. See Figure 69 for principle sketch.

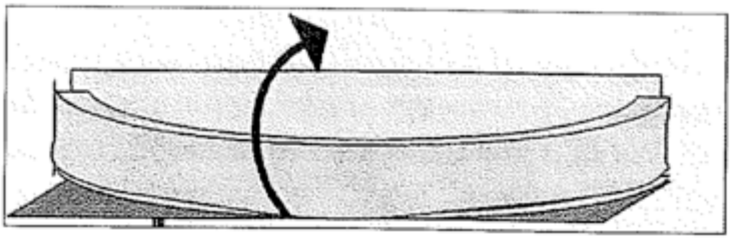

FIGURE 69: PRINCIPLE SKETCH VISOR GATE FRONT VIEW

Advantage:

- Maintenance can be performed above water

Disadvantage:

- Concentrated stress at the rotation points.
- Limited vertical clearance for navigation.
- Visual disturbance in opened position.

13.9 Barge gate

A barge gate is fixed at one side of the opening. It closes by rotating around the vertical axis of this fixed point, see Figure 70. Also here floating barge gates are preferred in order to reduce the hinge and operating force. It is possible to have wall openings with valves to keep it permeable during closure. This permeability allows better control over the barrier during rotation. After it is immersed and completely closed, the valves will be closed in order to make it water retaining.

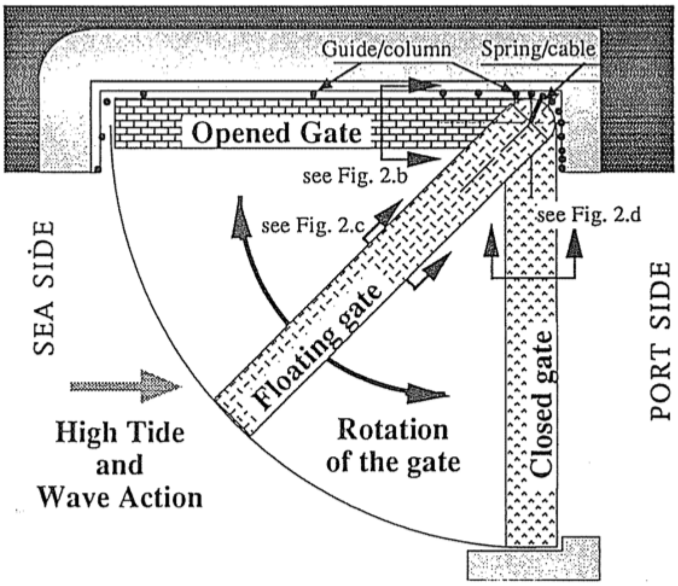

FIGURE 70: PRINCIPLE SKETCH BARGE GATE

Advantage
1. Unlimited vertical clearance when opened

Disadvantage
1. Big forces (water flow) work on gate during opening and closure
2. Large space need on the side where the gate is stored

14 APPENDIX 14: GEOMETRY DEFINITION FLOATING CAISSON

The will be separated into five parts, the central caisson and the two symmetrical abutments divided into two parts, one rectangular part and one trapezoid part, see Figure 71.

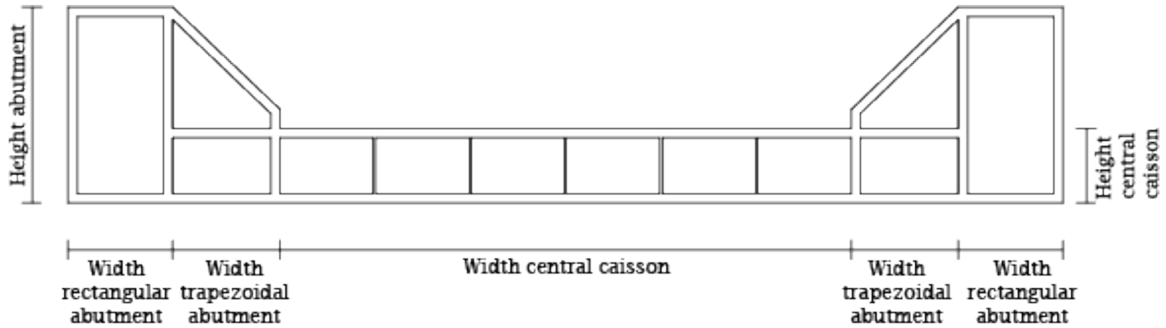

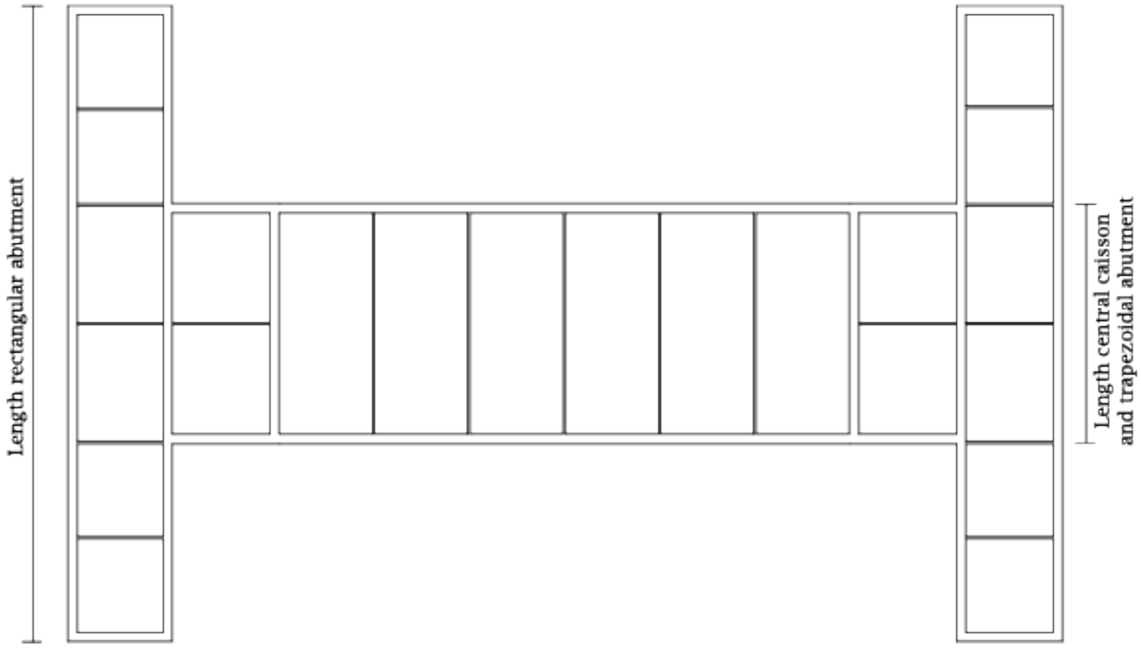

FIGURE 71: GEOMETRY FLOATING CAISSON

The geometries of the floating caisson are defined as following:

$$V_{cc} = W_{cc} * L_{cc} * H_{cc}$$
$$V_{cc,in} = W_{cc,in} * L_{cc,in} * H_{cc,in}$$
$$V_{ab,rec} = W_{ab,rec} * L_{ab,rec} * H_{ab,rec}$$
$$V_{ab,rec,in} = W_{ab,rec,in} * L_{ab,rec,,in} * H_{ab,rec,in}$$
$$V_{ab,tra} = (H_{ab,tra} + H_{cc} + H_{br}) * W_{ab,tra}/2 * L_{ab,tra}$$
$$V_{ab,tra,in} = (H_{ab,tra,in} + H_{cc,in} + H_{br}) * W_{ab,tra,in}/2 * L_{ab,tra,in}$$

with:

$$W_{cc} = W_{cc,in} + (n_{y,cc} - 1) * w_{cc,in}$$
$$L_{cc} = L_{cc,in} + 2 * w_{cc,out}$$
$$H_{cc} = H_{cc,in} + 2 * w_{slab}$$
$$W_{ab,rec} = W_{ab,rec,in} + w_{ab,out} + w_{ab,in}$$
$$L_{ab,rec} = L_{ab,rec,in} + \left(n_{x,ab,rec} - 1\right) * w_{ab,in} + 2 * w_{ab,out}$$
$$H_{ab,rec} = H_{ab,rec,in} + 2 * w_{slab}$$
$$W_{ab,tra} = W_{ab,tra,in} + w_{ab,out}$$
$$L_{ab,tra} = L_{fc,in} + \left(n_{x,ab,tra} - 1\right) * w_{fc,in} + 2 * w_{ab,out}$$
$$H_{ab,tra} = H_{fc,in} + 3 * w_{slab}$$

In which:

V_{cc}	[m^3]	Volume central caisson
W_{cc}	[m]	Width central caisson
L_{cc}	[m]	Length central caisson
H_{cc}	[m]	Height central caisson
H_{br}	[m]	Height bottom recess
$V_{cc,in}$	[m^3]	Total volume empty compartment central caisson
$W_{cc,in}$	[m]	Total width empty compartment central caisson
$L_{cc,in}$	[m]	Total length empty compartment central caisson
$H_{cc,in}$	[m]	Total height empty compartment central caisson
$V_{ab,rec}$	[m^3]	Volume rectangular part abutment
$W_{ab,rec}$	[m]	Width rectangular part abutment
$L_{ab,rec}$	[m]	Length rectangular part abutment
$H_{ab,rec}$	[m]	Height rectangular part abutment
$V_{ab,rec,in}$	[m^3]	Total volume empty compartment rectangular abutment
$W_{ab,rec,in}$	[m]	Total width empty compartment rectangular abutment
$L_{ab,rec,in}$	[m]	Total length empty compartment rectangular abutment
$H_{ab,rec,in}$	[m]	Total height empty compartment rectangular abutment
$V_{ab,tra}$	[m^3]	Volume trapezoid part abutment
$W_{ab,tra}$	[m]	Width trapezoid part abutment
$L_{ab,tra}$	[m]	Length trapezoid part abutment
$H_{ab,tra}$	[m]	Height trapezoid part abutment
$V_{ab,tra,in}$	[m^3]	Total volume empty compartment trapezoid part abutment
$W_{ab,tra,in}$	[m]	Total width empty compartment trapezoid part abutment
$L_{ab,tra,in}$	[m]	Total length empty compartment trapezoid part abutment
$H_{ab,tra,in}$	[m]	Total height empty compartment trapezoid part abutment
$w_{cc,in}$	[m]	Thickness inner wall central caisson
$w_{cc,out}$	[m]	Thickness outer wall central caisson
$w_{ab,in}$	[m]	Thickness inner wall abutment
$w_{ab,out}$	[m]	Thickness outer wall abutment
w_{slab}	[m]	Thickness top and bottom slab and inner floor
$n_{y,cc}$	[-]	Number of compartment central caisson (in width-direction)
$n_{x,ab,rec}$	[-]	Number of compartment rectangular abutment (in length-direction)
$n_{x,ab,tra}$	[-]	Number of compartment trapezoid abutment (in length-direction)

15 APPENDIX 15: STATIC FLOATING STABILITY NORMAL CONDITION

The stability of floating caissons is maintained by keeping the metacenter of the caisson above the gravity center of the caisson by a minimum of 0.5 m see Figure 72. In the figure, M is the metacenter, G is the gravity center, B is the center of buoyancy and K is the reference point.

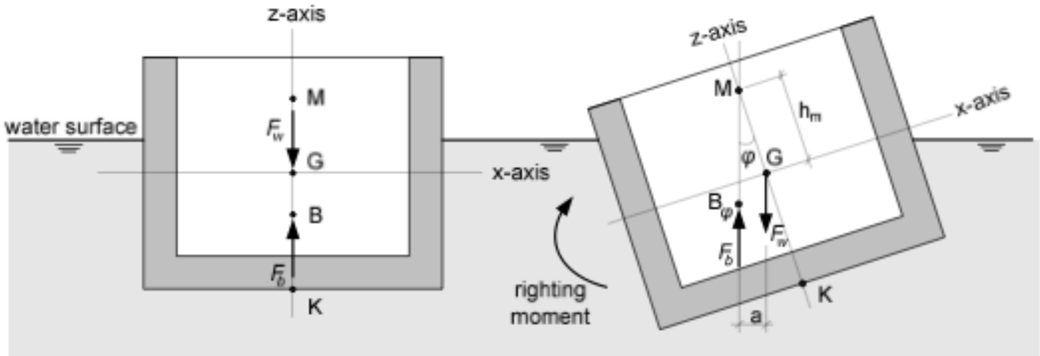

FIGURE 72: STATIC STABILITY SCHEME EMPTY CAISSON

The distance between the metacenter and the gravity center can be determined as follows:

$$GM = BM + KB - KG$$

Which:

$$BM = \frac{\min\{I_{xx,surface}, I_{yy,surface})}{V_{disp}}$$

$$KB = \frac{2 * \left(F_{ab,rec,disp} * e_{ab,rec,disp}\right) + 2 * \left(F_{ab,tra,disp} * e_{ab,tra,disp}\right) + F_{cc,disp} * e_{cc,disp}}{2 * F_{ab,rec,disp} + 2 * F_{ab,tra,disp} + F_{cc,disp}}$$

$$KG = \frac{2 * \left(F_{ab,rec} * e_{ab,rec}\right) + 2 * \left(F_{ab,tra} * e_{ab,tra}\right) + F_{cc} * e_{cc} + F_{ballast} * e_{ballast}}{2 * F_{ab,rec} + 2 * F_{ab,tra} + F_{cc,disp} + F_{ballast}}$$

$$V_{disp} = W_{cc} * L_{cc} * H_{cc} + 2 * D_c * W_{ab,rec} * L_{ab,rec} + 2 * (D_c * \left(H_{ab,tra} - D_c\right) + (D_c + H_{cc} + H_{br}) * (W_{ab,tra} - \left(H_{ab,tra} - D_c\right))/2) * L_{ab,tra}$$

$$I_{xx,surface} = 2 * \frac{1}{12} * W_{ab,rec} * L_{ab,rec}{}^{3} + 2 * \frac{1}{12} * \left(H_{ab,tra} - D_c\right) * L_{ab,tra}{}^{3} - 2 * \left(n_{y,ab,rec} * 2 * \left(W_{ab,rec,in} * \frac{L_{ab,rec,comp2}{}^{3}}{12} + W_{ab,rec,in} * L_{ab,rec,comp2} * \left(\frac{L_{ab,rec,comp2}}{2} + 0.5 * w_{ab,in}\right)^{2}\right)\right) - 2 * \left(n_{y,ab,rec} * 2 * \left(W_{ab,rec,in} * \frac{L_{ab,rec,comp1}{}^{3}}{12} + W_{ab,rec,in} * L_{ab,rec,comp1} * \left(L_{ab,rec,comp2} + L_{ab,rec,comp1} + 1.5 * w_{ab,in}\right)^{2}\right)\right) - 2 * \left(n_{y,ab,rec} * 2 * \left(W_{ab,rec,in} * \frac{L_{ab,rec,comp1}{}^{3}}{12} + W_{ab,rec,in} * L_{ab,rec,comp1} * \left(L_{ab,rec,comp2} + 1.5 * L_{ab,rec,comp1} + 2.5 * w_{ab,in}\right)^{2}\right)\right)$$

$$I_{yy,surface} = 2 * (\frac{1}{12} * L_{ab,rec} * W_{ab,rec}{}^{3} + \frac{1}{12} * L_{ab,tra} * \left(H_{ab,tra} - D_c\right)^{3} + L_{ab,rec} * W_{ab,rec} * \left(\frac{W_{cc} + W_{ab,rec}}{2} + \left(H_{ab,tra} - D_c\right)\right)^{2} + L_{ab,tra} * \left(H_{ab,tra} - D_c\right) * \left(\frac{W_{ab,rec} + \left(H_{ab,tra} - D_c\right)}{2}\right)^{2} - 4 * \frac{L_{ab,rec,comp1} * W_{ab,rec,in}{}^{3}}{12} - 2 * \frac{L_{ab,rec,comp2} * W_{ab,rec,in}{}^{3}}{12} - 4 * L_{ab,rec,comp1} * W_{ab,rec,in} * \left(\frac{W_{cc} + W_{ab,rec}}{2} + \left(H_{ab,tra} - D_c\right)\right)^{2} - 2 * L_{ab,rec,comp2} * W_{ab,rec,in} * \left(\frac{W_{cc} + W_{ab,rec}}{2} + \left(H_{ab,tra} - D_c\right)\right)^{2})$$

Where:

BM	[m]	Distance between metacenter and center of buoyancy
KB	[m]	Distance between center of buoyancy and reference point
KG	[m]	Distance between gravity center and reference point
$I_{xx,surface}$	[m^4]	Mass moment of inertia of the water cutting surface in x-direction
$I_{yy,surface}$	[m^4]	Mass moment of inertia of the water cutting surface in y-direction
V_{disp}	[m^3]	Displaced water volume by structure
$F_{ab,rec,disp}$	[kN]	Weight displaced water rectangular abutment ($V_{ab,rec}$* ρ_w)
$F_{ab,tra,disp}$	[kN]	Weight displaced water trapezoid abutment ($V_{ab,tra}$* ρ_w)
$F_{cc,disp}$	[kN]	Weight displaced water central caisson (V_{cc}* ρ_w)
$F_{ballast}$	[kN]	Weight ballast
$e_{ab,rec,disp}$	[m]	Distance between gravity central of displaced water by rectangular abutment part and reference point (0.5 * draught)
$e_{ab,tra,disp}$	[m]	Distance between gravity central of displaced water by trapezoid abutment part and reference point, see formula below.

$$e_{ab,tra,disp} = \frac{D_c * \left(H_{ab,tra} - D_c\right) * \frac{D_c}{2} + (D_c + H_{br} + H_{cc}) * \frac{(W_{ab,tra} - (H_{ab,tra} - D_c))}{2} * \frac{((H_{br} + H_{cc})^2 + (H_{br} + H_{cc}) * D_c + D_c^2}{3 * (D_c + H_{br} + H_{cc})}}{D_c * \left(H_{ab,tra} - D_c\right) + (D_c + H_{br} + H_{cc}) * \frac{(W_{ab,tra} - (H_{ab,tra} - D_c))}{2}}$$

$e_{cc,disp}$	[m]	Distance between gravity central of displaced water by central caisson and reference point (H_{cc}*0.5)
$e_{ab,rec}$	[m]	Distance between gravity central rectangular abutment and reference point ($H_{ab,rec}$*0.5)
$e_{ab,tra}$	[m]	Distance between gravity central trapezoid abutment and reference point (H_{fc}*0.5+w_{salb})

$$e_{ab,tra,disp} = \frac{\left(\left(H_{ab,tra} + H_{br} + H_{cc}\right) * \frac{W_{ab,tra}}{2} - \left(H_{ab,tra,in} + H_{br} + H_{cc,in} + w_{slab}\right) * \frac{W_{ab,tra,in}}{2}\right) * \frac{(W_{ab,tra} - (H_{ab,tra} - D_c))}{2} * \frac{((H_{br} + H_{cc})^2 + (H_{br} + H_{cc}) * D_c + D_c^2}{3 * (D_c + H_{br} + H_{cc})}}{\left(H_{ab,tra} + H_{br} + H_{cc}\right) * \frac{W_{ab,tra}}{2} - \left(H_{ab,tra,in} + H_{br} + H_{cc,in} + w_{slab}\right) * \frac{W_{ab,tra,in}}{2} + W_{ab,tra,in} * W_{ab,tra,in}}$$

e_{cc}	[m]	Distance between gravity central central caisson and reference point (H_{cc}*0.5)
$e_{ballast}$	[m]	Distance between gravity central ballast and reference point

16 APPENDIX 16: STATIC FLOATING STABILITY STORM SURGE CONDITION

The same method can be used to calculate to static stability of the structure under storm surge condition. The only difference compared to the normal condition is that the rubber dam is now inflated with water and air, leading to an upward shift of the gravity centre of the structure, making it unstable.

For the initial calculation of the storm surge situation, it is assumed the inflatable bellow is completely filled with water, which is the most unfavourable condition. To simplify initial calculation, the bellow is assumed to be a half cylinder over the whole span. KG is now:

$$KG = \frac{2 * (F_{ab,rec} * e_{ab,rec}) + 2 * (F_{ab,tra} * e_{ab,tra}) + F_{cc} * e_{cc} + F_{ballast} * e_{ballast} + F_{bellow} * e_{bellow}}{2 * F_{ab,rec} + 2 * F_{ab,tra} + F_{cc,disp} + F_{ballast} + F_{bellow}}$$

$$F_{bellow} = \frac{\pi * H_{bellow}^2}{2} - \frac{91.8}{360} * \pi * H_{bellow}^2 + 8 * 8.26 * \frac{W_{bellow,bot} + W_{bellow,top}}{2} * \rho_w$$

$$e_{bellow} = H_{bellow} - H_{bellow} * \frac{2 * W_{bellow,bot} + W_{bellow,top}}{3 * W_{bellow,bot} + W_{bellow,top}} + H_{cc}$$

Where:

F_{bellow}	[kN]	Weight water inside the bellow
e_{bellow}	[m]	Distance between gravity center bellow and reference point
H_{bellow}	[m]	Height inflatable rubber bellow
$W_{bellow,bot}$	[m]	Width bellow bottom
$W_{bellow,top}$	[m]	Width bellow top

17 APPENDIX 17: WATER LEVEL RISE DUE TO WAVE OVERTOPPING

The approximation used for the overtopping is the following (TU Delft, 2011):

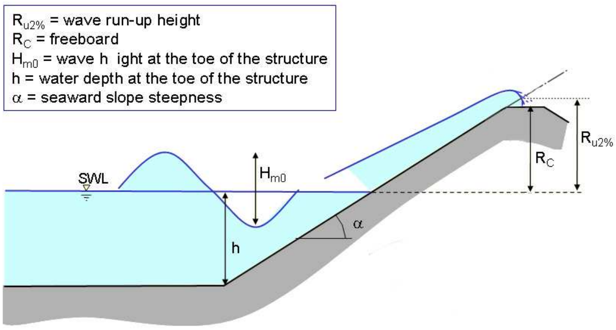

FIGURE 73: WAVE OVERTOPPING APPROXIMATION (TU DELFT, 2011)

$$\frac{q}{\sqrt{g * H_{m0}^3}} = a * e^{\frac{-b*R_c}{H_{m0}}}$$

$$a = \frac{0.067}{\sqrt{\tan(\alpha)}} * \gamma_b * \varepsilon_{m-1,0}$$

$$b = \frac{4.3}{\varepsilon_{m-1,0} * \gamma_b * \gamma_f * \gamma_\beta * \gamma_v}$$

$$\varepsilon_{m-1,0} = \frac{\tan(\alpha)}{\sqrt{\frac{H_{m0}}{1.56 * 0.9 * T_p}}}$$

Where:

q	[m³/s/m]	Overtopping discharge
R_c	[m]	Free board height (2.75 m for scenario storm condition rightcafter barrier construction and 1.75 m for scenario storm condition year 2100)
H_{m0}	[m]	Significant wave height (3.95 m)
T_p	[s]	Wave period (4.7 s, average value of the wave periods of The monthly maximum wave height recorded at Dai Ni Kaiho) (Independent Administrative Institution, Port and Airport institute)
Tan(α)	[-]	Slope steepness under water dam (assumed to be 1:3)
γ_b	[-]	Correction factor for present of a berm (absent)
γ_f	[-]	Correction factor for permeability and roughness of the slope (0.7)
γ_β	[-]	Correction factor for oblique wave attack, assumed perpendicular wave (1)
γ_v	[-]	Correction factor for vertical wall on top of crest

$$\gamma_v = 1.35 - 0.0078 * \alpha_{wall} = 1.35 - 0.0078 * 90 = 0.648$$

17.1.1.1.1 Scenario right after barrier construction

Filling in the formula gives an overtopping discharge of 0.017 m³/s/m, which results in a water level rise of:

$$0.003 * 6 * 3600 * \frac{6900}{920000000} = 0.0004m$$

17.1.1.1.2 Scenario year 2100

Filling in the formula gives an overtopping discharge of 0.23 m³/s/m, which results in a water level rise of:

$$0.04 * 6 * 3600 * \frac{6900}{920000000} = 0.006m$$

18 APPENDIX 18: LOADS CALCULATION

This paragraph considers the loads that are taken into account for the calculation of the mooring lines. For the design of mooring lines three load cases are considered, which are the typhoon load case, the tsunami load case and the earthquake load case.

18.1.1.1 Typhoon load case

In this section the load on the floating barrier during the design typhoon condition. This load case consists the hydrostatic load caused by the storm surge and the wave load. Since the largest water head is generated during storm condition in year 2100, it has been recognized at the governing condition for the load determination for the typhoon load case.

18.1.1.1.1 Horizontal load

Hydrostatic load

The schematic view of the considered horizontal hydrostatic loads is shown in Figure 74.

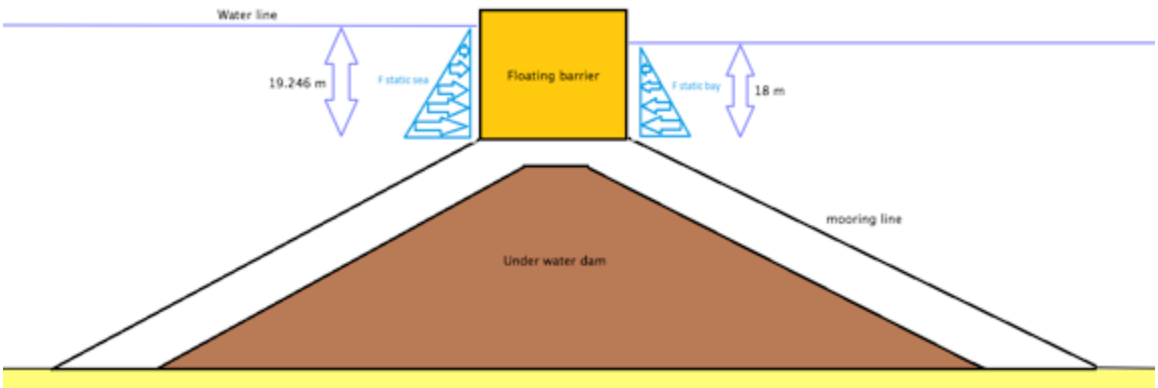

FIGURE 74: SCHEMATIC VIEW HYDROSTATIC LOAD

The hydrostatic load can be calculated with:

$$F_{static,h} = 0.5 * \rho * g * h^2 * B$$

Where:

$F_{static,h}$	[m]	Horizontal hydrostatic force per barrier
h	[m]	Draught in front (19.246 m) and back (18 m) of the floating barrier
B	[m]	Width of the floating barrier (106.75 m)

Filling in the formula gives

TABLE 15: HORIZONTAL HYDROSTATIC LOADS ON THE FLOARING BARRIER

$F_{static,h,sea}$	193950 kN/barrier
$F_{static,h,bay}$	169650 kN/barrier

Wave loads

Before the wave load can be calculated, it has to be determined whether the wave will break at the barrier. This can be done using the following thumb rules, the wave will break if:

$$H/L \geq 1/7$$

or

$$H/d \geq 0.78$$

Where:

H	[m]	Design wave height
L	[m]	Wave length design wave
d	[m]	Water depth

Filling these criteria with the design wave properties gives:

$$\frac{H}{L} = \frac{3.95}{4.7 * \sqrt{9.81 * 3.95}} = 0.135 < 1/7$$

and

$$\frac{H}{d} = \frac{3.95}{21} = 0.19 < 0.78$$

Therefore it can be concluded that the design wave won't break at the barrier.

For the calculation of the wave loads, the Goda theory (Goda, 1985) is used. This is because the assumed situation by Goda is in some way similar to the situation of this research. The under water dam can be approximated by the sill assumed in the theory. However the gap between the dam and the floating barrier is absent in the scheme given by Goda, but it is assumed that the influence of this gap on the wave force of the floating barrier is negligible small. The schematic view of Goda is shown in Figure 75

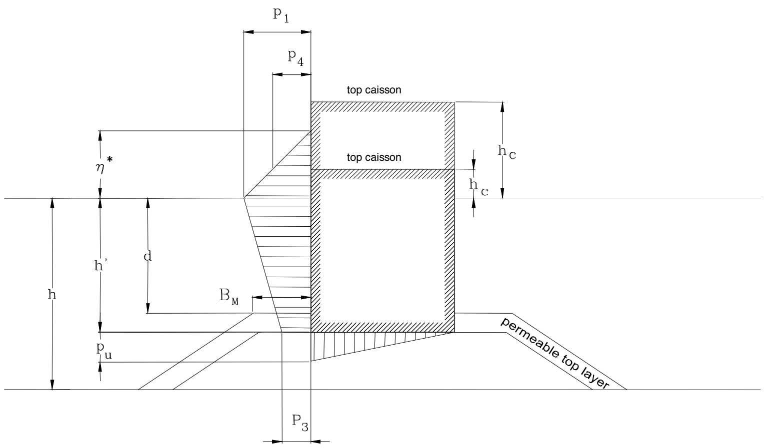

FIGURE 75: SCHEMATIC VIEW GODA THEORY (TU DELFT, 2011)

The maximum wave pressures are:

$$P_1 = 0.5(1 + \cos(\beta))(\lambda_1\alpha_1 + \lambda_2\alpha_2 cos^2(\beta))\rho g H_D$$
$$P_3 = \alpha_3 P_1$$
$$P_4 = \alpha_4 P_1$$

In which:

$\eta = 0.75(1 + \cos(\beta))\lambda_1 H_D$

$\alpha_1 = 0.6 + 0.5\left(\frac{\frac{4\pi h}{L_D}}{\sinh\left(\frac{4\pi h}{L_D}\right)}\right)^2$

$$\alpha_3 = 1 - (\frac{h'}{h})\left(1 - \frac{1}{\cosh\left(\frac{2\pi h}{L_D}\right)}\right)^2$$

$$\alpha_4 = 1 - \frac{h'_c}{\eta}$$

$h'_c = \min(\eta, h_c)$

β	[degree]	The angle of the incoming wave (0, front wave)
$\lambda_1, \lambda_2, \lambda_3$	[-]	Factors dependent on the shape of the structure and on wave conditions; (straight wall and non-breaking waves: λ_1=λ_2=λ_3=1)
h_b	[m]	Water depth at a distance $5H_D$ from the wall
H_D	[m]	Design wave height (3.95 m)
L_D	[m]	Design wave length

$$L_D = T_p\sqrt{g * H_D} = 4.7 * \sqrt{9.81 * 3.95} = 29.26\,m$$

d	[m]	Water depth above the top of the sill (draught floating barrier, 18 + 1.246 = 19.246m)
h'	[m]	Water depth above the wall foundation plain (draught floating barrier, 18 + 1.246 = 19.246m)
h	[m]	Water depth in front of the sill, assumed navigation channel Is at the deepest part of the span, which is 81 m. The depth at the location of the floating barrier of this preliminary design is assumed to be the depth right next to the navigation channel, which is 72 m, that is where the largest wave force will occur.

Filling in the formulas gives:

$$P_1 = 23.6\,kN/m^2$$
$$P_3 = 17.3\,kN/m^2$$
$$P_4 = 11.7kN/m^2$$

$$F_{wave,h} = \left((P_1 + P_3) * \frac{d}{2} + (P_1 + P_4) * \frac{h'_c}{2}\right) * B$$
$$= ((23.6 + 17.3) * \frac{19.246}{2} + (23.6 + 11.7) * \frac{1.754}{2}) * 106.75$$
$$= 45225\,kN/barrier$$

Resultant horizontal force

The resultant horizontal force on the floating barrier from the hydrostatic load and wave load is the:

$$F_{static,h,sea} + F_{wave,h} - F_{static,h,bay} = 193950 + 45225 - 169650 = 69525\,kN/barrier$$

18.1.1.1.2 Vertical load

The vertical load is determined for the moment when the storm surge on the sea side is at its maximum level, where probably the maximum wave height will occur.

Hydrostatic load

The schematic view of the considered vertical hydrostatic loads is shown in Figure 74.

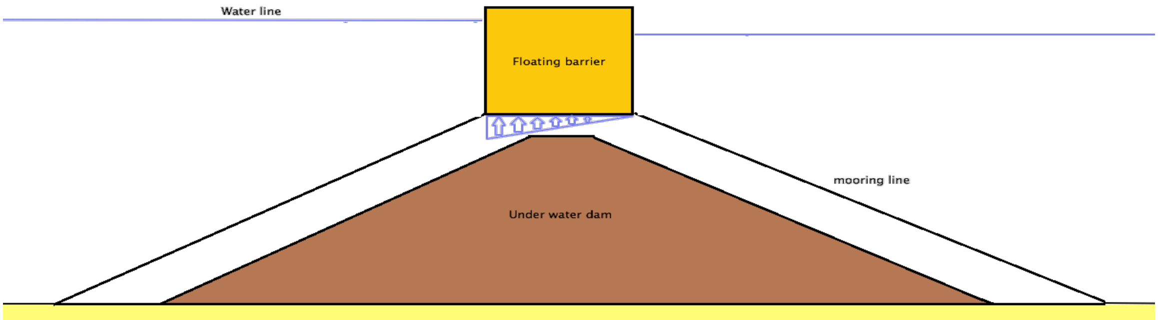

FIGURE 76: SCHEMATIC VIEW VERTICAL HYDROSTATIC LOAD

The vertical hydrostatic load can be calculated with:

$$F_{static,v} = 0.5 * \rho * g * h * (2 * (L_{ab,rec} * B_{ab,rec} + L_{ab,tra} * B_{ab,tra}) + L_{cc} * L_{cc})$$

Where:

$F_{static,v}$	[m]	Vertical hydrostatic force per barrier
h	[m]	Extra draught compared to the design draught at sea side of the floating barrier (1.246 m)
$L_{ab,rec}$	[m]	Length of the rectangular abutment of the floating barrier
$B_{ab,rec}$	[m]	Width of the rectangular abutment of the floating barrier
$L_{ab,tra}$	[m]	Length of the trapezoidal abutment of the floating barrier
$B_{ab,tra}$	[m]	Width of the trapezoidal abutment of the floating barrier
L_{cc}	[m]	Length of the central caisson of the floating barrier
B_{cc}	[m]	Width of the central caisson of the floating barrier

Filling in the equation gives:

$$F_{static,v} = 29180\ kN/barrier$$

Wave load

The schematic view of the considered vertical wave loads is shown in Figure 74.

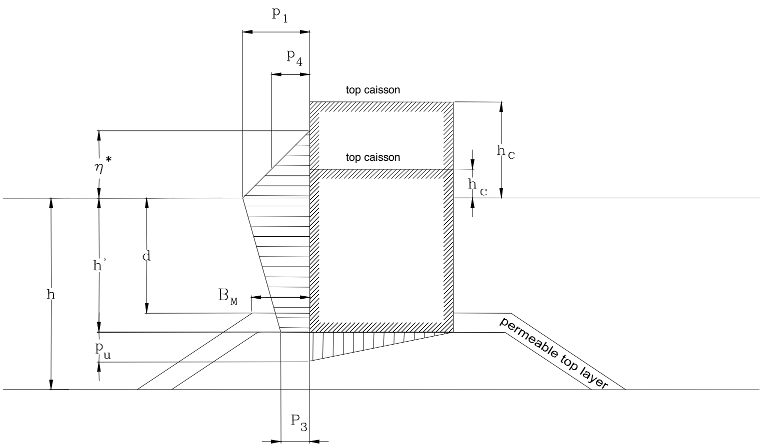

FIGURE 77: SCHEMATIC VIEW WAVE LOAD (TU DELFT, 2011)

The maximum vertical wave pressure is the same as the P_3 value calculated for the Goda approximation (Goda, 1985) in the previous paragraph, which is 17.3 kN/m². The vertical load caused by the wave can be calculated with:

$$F_{wave,h} = 0.5 * P_3 * (2 * (L_{ab,rec} * B_{ab,rec} + L_{ab,tra} * B_{ab,tra}) + L_{cc} * L_{cc}) = 41202\ kN/barier$$

Resultant vertical force

The resultant force on the floating barrier from the hydrostatic load and wave load is the:

$$F_{static,v,} + F_{wave,v} = 29180 + 41202 = 70382\ kN/barrier$$

18.1.1.2 Tsunami load case

In this section the load on the floating barrier due to tsunami will be calculated. Since the chance of the tsunami and typhoon to occur at the same time is considered to be negligible small, only the tsunami wave load will be considered for the tsunami load case.

First it will be checked whether the tsunami wave will break during impact at the barrier. Bryant (Bryant, 2001) presents a breaking criterion for tsunami waves on a slope, see equation below. The tsunami wave will break when B_r becomes larger than 1.

$$B_r = \frac{\varpi^2 * H}{g * tan^2\beta}$$

Where:

ϖ	[rad/s]	The angular frequency, $\varpi = \frac{2\pi}{T}$
β	[degree]	Slope of the sea bed, assumed to be 1:100, which is 0.57 degrees.
H	[m]	Tsunami wave height (0.8 m)

To be able to calculate the angular frequency of the tsunami wave, the tsunami wave period needs to be determined first using the tsunami wave length. Typical tsunami wavelengths for different water depths are shown in Figure 78.

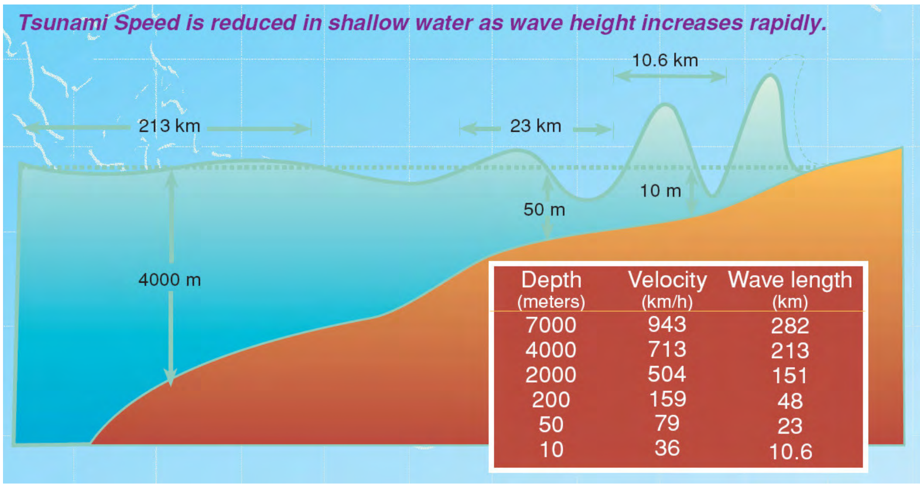

Depth (meters)	Velocity (km/h)	Wave length (km)
7000	943	282
4000	713	213
2000	504	151
200	159	48
50	79	23
10	36	10.6

FIGURE 78: TYPICAL PARAMETERS FOR TSUNAMI WAVES (PLAS, 2007)

As it can be seen from Figure 78, for a average water depth of 50 m the corresponding tsunami wave length is approximately 23 km. Since the tsunami wave height is much smaller than this tsunami wave length (H/L < 1/20), the tsunami wave can be considered as shallow water waves. Therefor the wave period 'T' of the tsunami can be determined using the following formula:

$$T = \frac{L}{\sqrt{g * H}} = \frac{23000}{\sqrt{9.81 * 0.8}} = 8210\ s$$

Filling in the equation presented by Bryant gives:

$$B_r = \frac{\varpi^2 * H}{g * tan^2\beta} = \frac{\left(2 * \frac{\pi}{8210}\right)^2 * 0.8}{9.81 * tan^2(0.57)} = 0.0005$$

Since the obtained B_r value is smaller than 1, it can be concluded that tsunami wave won't break at the barrier location.

The tsunami wave load will be calculated with the formula proposed by Tanimoto (Tanimoto, 1981), see Figure 79.

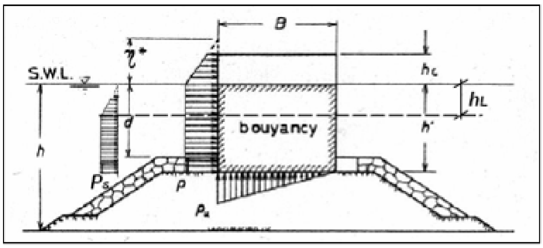

FIGURE 79: WAVE PRESSURE DISTRIBUTION DUE TO NON-BREAKING LONG-PERIOD WAVES (TANIMOTO, 1981)

The horizontal wave force per meter width P and uplift force per meter width Uare expressed as follows:

$$P = \{1 + \left(1 - \frac{h_c^*}{3H}\right)\frac{h_c^*}{h'}\}ph'$$

$$U = \frac{1}{2}p_u B$$

Where:

η^* [m] The height above the still water level at which the pressure is zero

$$\eta^* = 1.5H = 1.5 * 0.8 = 1.2\ m$$

p [kN/m²] The wave pressure intensity which acts uniformly on the vertical wall below the still water level

p_u [kN/m²] The uplift pressure.

$$p = p_u = 1.1 * \rho_w * H = 1.1 * 9.81 * 1000 * \frac{0.8}{1000} = 8.6328\ kN/m^2$$

h_c^* [m] min{η^*, h_c)

Filling in the equation and by multiplying it with the corresponding barrier width gives:

Horizontal force	11721 kN/barrier
Vertical force	20609 kN/barreir

18.1.1.3 Earthquake load

The earthquake load on the mooring lines is equal to the ground surface acceleration multiplied with the mass of the floating barrier plus the friction caused by the water. Since the determination of the exact friction on the floating barrier is a rather complex process, the earthquake load will be checked without water friction first to get a feeling of the magnitude of the load. The assumed earthquake acceleration is 0.5 m/s^2 (Shima, Komiya, & Tonouchi, 1988). This is the maximum acceleration measured during the great Kanto earthquake in 1923 (M8.0), which has the same magnitude as the assumed design earthquake in chapter 5.2.6 of the main report. This acceleration is assumed for both horizontal and vertical loads.

$$F_e = m * a = 5 * 10^7 * \frac{0.5}{1000} = 2.8 * 10^4 \; kN$$

Since this load is well below the load caused by the typhoon load case, it is believed that even taken into account the contribution of the water friction, the load caused during earthquake will still be well below the load generated during the design typhoon.

19 APPENDIX 19: EQUATIONS OF MOTION FLOATING BARRIER

By using the displacement method, forces on the floating barrier during the different motions can be determined. These motions are given in Figure 80 to Figure 85. For each motion, the equation of motion is also given (without earthquake load). The positive motion directions are indicated by the given axis directions. Note that the mooring chains can only contain tension, this is approximated by modelling the springs in the x and y direction acting only in the direction when it is tensioned. Springs in the z-direction are modelled as normal springs that act when both compressed and tensioned. This is due to the non-linearity and inconsistency these z-directional springs give to the system.

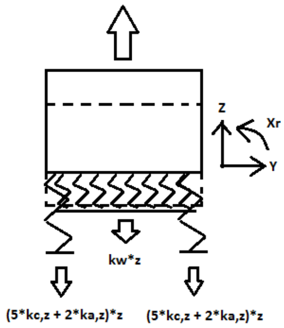

FIGURE 80: MOTION IN Z-DIRECTION

$$M * \ddot{x} + \left(10 * k_{c,z} + 4 * k_{a,z}\right) * z + k_w * z = 0$$

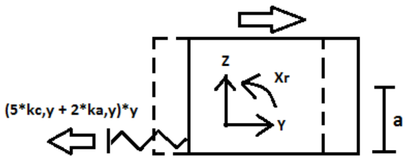

FIGURE 81: MOTION IN Y-DIRECTION

$$M * \ddot{x} + \left(5 * k_{c,y} + 2 * k_{a,y}\right) * y + \left(5 * k_{c,y} + 2 * k_{a,y}\right) * x_r * a = 0$$

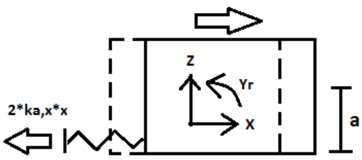

FIGURE 82: MOTION IN X-DIRECTION

$$M * \ddot{x} + 2 * k_{a,x} * x + 2 * k_{a,x} * y_r * a = 0$$

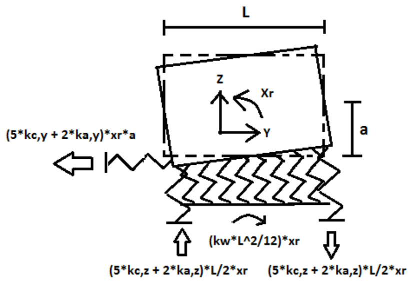

FIGURE 83: MOTION IN XR-DIRECTION

$$J1 * \ddot{x}_r + \frac{k_w}{12} * L^2 * x_r + (5 * k_{c,y} + 2 * k_{a,y}) * a * y + (5 * k_{c,z} + 2 * k_{a,z}) * x_r * \frac{L^2}{4} + (5 * k_{c,y} + 2 * k_{a,y}) * x_r * a^2 = 0$$

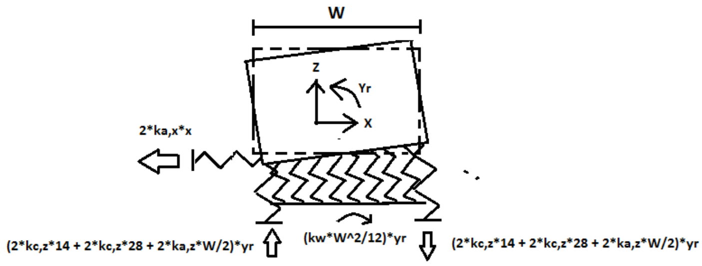

FIGURE 84: MOTION IN YR-DIRECTION

$$J2 * \ddot{y}_r + 2 * k_{a,x} * x * a + \frac{k_w}{12} * W^2 * y_r + (2 * 14^2 + 2 * 28^2) * k_{c,z} * y_r + 2 * \frac{W^2}{4} * k_{a,z} * y_r = 0$$

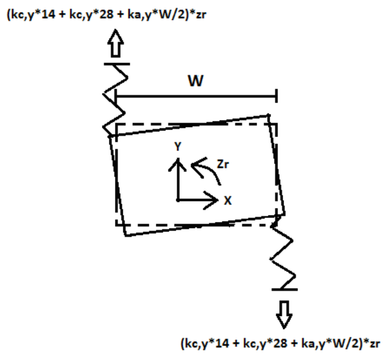

FIGURE 85: MOTION IN ZR-DIRECTION

$$J3 * \ddot{z}_r + (2 * 14^2 + 2 * 28^2) * k_{c,y} * z_r + 2 * k_{a\,y} * \frac{W^2}{4} * z_r = 0$$

LIST OF FIGURES

LIST OF TABLES